Simulating the dynamical friction force on ions due to a briefly co-propagating electron beam

George I. Bell [a,*], David L. Bruhwiler [a], Alexei Fedotov [b], Andrey Sobol [a], Richard S. Busby [a], Peter Stoltz [a], Dan T. Abell [a], Peter Messmer [a], Ilan Ben-Zvi [b], Vladimir Litvinenko [b]

[a] Tech-X Corporation, Accelerator Technology, 5621 Arapahoe Avenue, Suite A, Boulder, CO 80303, United States
[b] Brookhaven National Lab, Upton, NY 11973, United States

ABSTRACT

We present two algorithms for accurate beam-frame simulations of the dynamical friction force on a non-relativistic ion moving for a short time in a low-density electron distribution, in the presence of arbitrary external fields. A special-purpose 4th-order predictor–corrector ("Hermite") algorithm, taken from the astrophysical dynamics community, has been generalized to work with charged particles in the presence of a constant magnetic field. An alternative algorithm uses operator splitting techniques to solve binary Coulomb collisions (BCC) in the presence of arbitrary external fields. We discuss the close mathematical relationship between the Hermite and BCC algorithms, and their order of convergence. We discuss the parallel efficiency of the BCC algorithm and use it in the parallel simulation framework VORPAL to study problems in a parameter regime relevant to the electron cooling section for the proposed luminosity upgrade of the Relativistic Heavy Ion Collider. In particular, we simulate the field-free case to show how finite time effects strongly modify the traditional Coulomb logarithm, resulting in a significant reduction of the dynamical friction force as calculated by standard theoretical formulas. We show that diffusive dynamics can be correctly simulated, but that it must be artificially suppressed in order to accurately obtain the friction force. We discuss the proposed use of a helical undulator magnet to focus the electron beam and inhibit electron–ion recombination, showing that this device reduces the friction force.

© 2008 Elsevier Inc. All rights reserved.

1. Introduction

Novel electron-hadron collider concepts are a high priority for the long-term plans of the international nuclear physics community. Orders of magnitude higher luminosity will be required for the relativistic ion beams in such particle accelerators. Higher luminosity can only be achieved by some dissipative mechanism that reduces the effective phase space volume occupied by the ion beam. A promising technique for this purpose, known as electron cooling, propagates an overlapping electron beam with the same velocity as the ions, for a small fraction of the collider circumference, allowing the ions to give up some of their thermal kinetic energy via Coulomb collisions. This very brief and subtle interaction provides weak damping of the effective ion phase space volume (i.e. cooling), which accumulates turn by turn to successfully combat a variety of mechanisms that increase this volume.

---

* Corresponding author. Tel.: +1 720 974 1857; fax: +1 303 448 7756.
  E-mail address: gibell@txcorp.com (G.I. Bell).

Electron cooling has been used successfully at many low-energy ion accelerator facilities around the world, using non-relativistic DC electron beams, in a strong solenoidal magnetic field [21,23,26]. This is referred to as "magnetized cooling," because the electrons are strongly coupled to the magnetic field lines, which greatly increases the friction force by suppressing the transverse electron temperature. At higher energies, much stronger solenoidal fields are required to magnetize the electrons, which eventually becomes impractical. It has recently been demonstrated [24] that electron cooling can work with a moderately relativistic electron beam, in a solenoidal field that is sufficiently strong to focus the electron beam but not result in magnetized electron dynamics. This is now referred to as "unmagnetized cooling".

The electron cooler for the proposed luminosity upgrade of RHIC [4,13] represents a significant design challenge due to the high energy of the ion beam. While lower energy ion beams can be cooled by continuous electron beams, the 55 MeV electron beam needed by RHIC must be a bunched beam, with consequently higher temperature electrons. In addition the long ion bunch length implies that only a small portion of the beam will overlap the electrons during one interaction. The requirements for an electron cooler are tight enough that, if cooling estimates are off by a factor of two, the cooling will not be sufficient to combat emittance growth from intra-beam scattering. Thus, careful estimates of dynamical friction from numerical simulations are critical for the proposed RHIC electron cooler.

We present two algorithms for non-relativistic, electrostatic simulations of the dynamical friction force exerted by a distribution of electrons on an individual ion. In particular, we consider the parameter regime of the proposed RHIC high-energy cooler. The original cooler design adopted the magnetized cooling approach. We provide details on the "Hermite" algorithm used in this case, a 4th-order predictor–corrector integration scheme, originally only valid for the field-free case, but generalized to work with charged particles in a magnetic field that is constant in both time and space. Simulations using the Hermite algorithm have previously [6,14,15] resolved discrepancies between alternate theoretical models for the magnetized friction force.

A more recent RHIC cooler design replaces the solenoid with a helical undulator magnet to provide transverse focusing of the electron beam and, by driving small-amplitude oscillations in the electron trajectories, reduce the ion-electron recombination rate. The undulator-driven electron oscillations reduce the friction force that would occur in the absence of external fields. When the helical undulator field is Lorentz-transformed into the beam-frame, one obtains rapidly-varying electric and magnetic fields, which cannot be accurately modeled with the Hermite algorithm. For this case we have developed an alternate algorithm, which uses an operator-splitting approach to combine a semi-analytic model for binary Coulomb collisions (BCC) between electron/ion pairs with a modified Boris push [5] to incorporate arbitrary external fields.

We present both algorithms in detail, showing that they are more closely related than one would initially expect, and we prove their order of convergence. Both algorithms have been implemented in the parallel simulation framework VORPAL [25]. Simulation results from using the BCC algorithm are presented here, both for the field-free case and in the presence of a helical undulator magnet.

1.1. Review of the friction force and the Coulomb logarithm

Calculation of the dynamical friction force in an "ideal" or "weakly coupled" electron plasma dates back to the work of Chandrasekhar in 1942 [9] and Trubnikov in 1965 [28]. The calculation can now be found in texts on basic plasma physics (e.g. Ref. [8]). For plasma applications, researchers typically assume a scalar temperature for the electrons. Our interest here is in relativistic electron beams, which in the beam-frame have a longitudinal temperature that is much lower than the transverse temperature. Derbenev [10] considers such complications, and also discusses the relationship between the friction force and diffusive dynamics. Budker [7] first recognized that the friction force provided a mechanism for cooling heavy ion beams by co-propagating them for a finite distance with lower temperature electron beams.

Finite time effects in a real electron cooling system can severely constrain the minimum and maximum impact parameters that are used in the standard Coulomb logarithm, leading to significantly weaker friction forces than are predicted by the usual theory. These finite time effects are calculated in later sections, but it is helpful to first review the standard derivation and to consider details regarding the approximate treatment of small impact parameters. This review follows the online text of Callen [8].

The friction force calculation assumes that binary Coulomb collisions dominate and that 3-body or higher n-body collisions can be ignored. This assumption is, essentially, the defining characteristic of an ideal or weakly-coupled plasma. This approximation is central to the simulations and analysis in the present work and, in particular, to the numerical trick (described below) of using correlated electron/positron pairs to suppress the diffusive motion of an ion. At the end of Appendix A, arguments based on Poisson statistics are used to clarify conditions under which this assumption is valid. In this appendix, a similar analysis is used to calculate the cutoff impact parameter which can be reasonably sampled in a finite time, called ρ_c.

The standard friction force calculation proceeds by integrating the Coulomb force on an electron as it follows an assumed straight-line trajectory past an ion. For this perturbative calculation, the impact parameter and the distance of closest approach are identical. By conservation of momentum, the force on the ion is equal and opposite. One then must integrate over all impact parameters, but this diverges logarithmically for both large and small impact parameters. To resolve this mathematical difficulty, one chooses physically reasonable values for $\rho_{\min}$ and $\rho_{\max}$, and limits the integration to this range. The standard Coulomb logarithm is defined to be the log of the ratio of these impact parameters:

$$\Lambda_0 = \int_{\rho_{\min}}^{\rho_{\max}} \frac{\mathrm{d}\rho}{\rho} = \ln\left(\frac{\rho_{\max}}{\rho_{\min}}\right). \tag{1}$$

The analysis is accurate in the limit that $\rho_{\max} \gg \rho_{\min}$, such that $\Lambda_0 \gg 1$, with errors of order $1/\Lambda_0$.

The divergence at large impact parameter is due to the long-range nature of the Coulomb force and the assumption that every electron/ion collision has an arbitrarily long time interval to complete. For interaction times τ long compared to the plasma period, one has $\tau\omega_{\mathrm{pe}} \gg 2\pi$, where $\omega_{\mathrm{pe}} = (n_e e^2/\epsilon_0 m_e)^{1/2}$ is the electron plasma frequency, n_e the electron density, e and m_e are the electron charge and mass, ϵ_0 is the permittivity of free space, and we are using MKS units. In this limit, for ion velocities $\mathbf{v}_{\mathrm{ion}}$ less than the (assumed isotropic) electron thermal velocity Δ, the electrons have time to form a higher-density cloud around the ion. At distances larger than the Debye length, $\lambda_D = \Delta/\omega_{\mathrm{pe}}$, the ion charge is completely shielded and electrons do not scatter. Hence, one typically chooses $\rho_{\max} = \lambda_D$. The case of ion velocities much larger than the thermal electron velocity is more complicated [29,30].

For the electron cooling parameters proposed for RHIC, we must work in the opposite limit, where $\omega_{\mathrm{pe}}\tau < 2\pi$. In this limit, there is essentially no shielding of the ion charge and $\rho_{\max}$ is limited only by some relatively large length scale, such as the beam radius. However, in this limit one must explicitly account for the finite interaction time, which leads to a modified form of the Coulomb logarithm and no singularities. These finite time effects are discussed in Section 7, resulting in the modified Coulomb logarithm in Eq. (37).

The impact parameter for 90° scattering is given by

$$\rho_{\min}(\mathbf{v}_{\mathrm{rel}}) = \frac{|k|}{m_e|\mathbf{v}_{\mathrm{rel}}|^2}, \tag{2}$$

where $\mathbf{v}_{\mathrm{rel}} = \mathbf{v}_{\mathrm{ion}} - \mathbf{v}_e$ is the relative velocity vector, $\mathbf{v}_{\mathrm{ion}}$ and $\mathbf{v}_e$ are the ion and electron velocities, respectively, and $k = Ze^2/(4\pi\epsilon_0)$, where Z is the ion charge number. Our convention is to use $k > 0$ for attracting particles and $k < 0$ for repelling particles. For collisions between particles of similar mass, we would replace the electron mass m_e by the reduced mass. The standard perturbative calculation of friction force breaks down at small impact parameters, and it is common to ignore all collisions with impact parameter less than $\rho_{\min}$. A more careful consideration of small impact parameter collisions will result in a modification of the Coulomb logarithm. We will see that it is important to distinguish between $\rho_{\min}$, a length defined by the particle's mass, charge, and relative velocity, and ρ_c, the smallest impact parameter that occurs.

Above, we have defined $\rho_{\min}$ to be a function of the relative velocity between a single ion and a single electron. It would then follow that the Coulomb logarithm defined above in Eq. (1) is also a function of this particular relative velocity. However, when a particular value of $\rho_{\min}$ is specified in the literature, most often the author has assumed an isotropic thermal plasma and replaced $\mathbf{v}_{\mathrm{rel}}$ with the rms electron velocity Δ.

The electron distribution most often considered by the electron cooling community is an accelerated beam in the co-moving reference frame, for which the transverse rms electron velocities (i.e. $\Delta_x = \Delta_y$) are much larger than the longitudinal rms velocity Δ_z. In such cases, one can integrate over the beam-frame electron velocity distribution $f(\mathbf{v}_e)$ to produce an average minimum impact parameter:

$$\rho_{\min}^{\mathrm{avg}} = \int_{-\infty}^{\infty} \rho_{\min}(\mathbf{v}_{\mathrm{rel}})f(\mathbf{v}_e)\mathrm{d}^3\mathbf{v}_e, \tag{3}$$

or else replace $\mathbf{v}_{\mathrm{rel}}$ with some weighted average of the three Δ_α values. In some cases, the typical ion velocity in the co-propagating ion beam may be large compared to some or all of the Δ_α, in which case the ion velocity in $\mathbf{v}_{\mathrm{rel}}$ is treated carefully in the integral above, or $\mathbf{v}_{\mathrm{rel}}$ is sometimes replaced with $\mathbf{v}_{\mathrm{ion}}$.

When a particular value is specified for the Coulomb logarithm Λ_0 in the literature, the authors are often using Eq. (1), with $\rho_{\min}$ defined in one of the various ways just described, although different segments of the plasma physics community have established various conventions for approximately calculating Λ_0. Alternatively, one can use the explicit form from Eq. (2) in Eq. (1), and then use this $\Lambda(\mathbf{v}_{\mathrm{rel}})$ inside an integral over the electron distribution.

The ensemble average friction force on an ion moving with velocity $\mathbf{v}_{\mathrm{ion}}$ through a cold electron distribution is [8]

$$\mathbf{F}_\parallel = 2\pi n_e m_e \mathbf{v}_{\mathrm{ion}} \int_{\rho_c}^{\rho_{\max}} \rho \delta v_\parallel \mathrm{d}\rho, \tag{4}$$

where $\delta v_\parallel$ is the change in the ion velocity parallel to $\mathbf{v}_{\mathrm{ion}}$ induced by a single collision. The parameter ρ_c is the lower limit or "cutoff" on impact parameter. which can be set to 0 to include all small impact parameter collisions.

As the impact parameter decreases, collisions corresponding to this impact parameter become less frequent. Hence, in any finite interaction time, with finite electron density, there is some impact parameter ρ_c, below which the number of collisions is too small to reasonably sample the $4\pi sr$ of interaction angles, so such impact parameters do not contribute to the friction force. This is explained in detail in Appendix A, where we calculate ρ_c. The parameter ρ_c is distinct from $\rho_{\min}$, and it is important not to confuse the two.

To obtain the friction force in a warm electron plasma, one replaces $\mathbf{v}_{\mathrm{ion}}$ with $\mathbf{v}_{\mathrm{rel}}$ and integrates over the electron distribution function, as is done below in Eq. (8). We can obtain an exact expression for $\delta v_\parallel$ using the standard Rutherford scattering formula for the scattering angle ϕ [8,20] (see also Appendix B),

$$\tan\frac{\phi}{2} = \pm\frac{\rho_{\min}}{\rho}, \tag{5}$$

with the sign determined by the sign of k (attracting vs. repelling charges), and $\rho_{\min}$ given by Eq. (2). The only assumption made in Eq. (5) is that the interaction time is infinite. Since $\delta v_{\parallel} =| \mathbf{v}_{\text{rel}} | (\cos\phi - 1)$, we find

$$\delta v_{\parallel} = -\frac{2|\mathbf{v}_{\text{rel}}|\rho_{\min}^2}{\rho^2 + \rho_{\min}^2} = -\frac{2k^2}{m_{\text{e}}^2|\mathbf{v}_{\text{rel}}|^3}\frac{1}{\rho^2 + \rho_{\min}^2}, \tag{6}$$

and integrating from ρ_{c} to $\rho_{\max}$ gives the total friction force

$$\mathbf{F}_{\parallel} = -\frac{4\pi n_{\text{e}}k^2\mathbf{v}_{\text{rel}}}{m_{\text{e}}|\mathbf{v}_{\text{rel}}|^3}\underbrace{\frac{1}{2}\ln\left(\frac{\rho_{\max}^2 + \rho_{\min}^2}{\rho_{\min}^2 + \rho_{\text{c}}^2}\right)}_{\Lambda_1}. \tag{7}$$

When $\rho_{\text{c}} = 0$ and $\rho_{\min} \ll \rho_{\max}$, Λ_1 is very close to the usual Coulomb logarithm Λ_0 in Eq. (1). For $\rho_{\text{c}} = 0$ and $\Lambda_0 > 2$, the relative error between Λ_1 and Λ_0 is less than 0.5%. But for a finite value of ρ_{c}, Λ_0 and Λ_1 will differ.

Somewhat surprisingly, in a perturbative setting involving only weak collisions ($\rho \gg \rho_{\min}$) we can derive Eq. (7) where Λ_0 replaces Λ_1 [8]. For a weak collision, $\delta v_{\parallel}$ is given by Eq. (6) with the denominator $\rho^2 + \rho_{\min}^2$ replaced by ρ^2. The integral in Eq. (4) now diverges for small impact parameters, but if we begin the integration from $\rho_{\min}$ we obtain Eq. (7) with Λ_1 replaced by Λ_0.

The standard Coulomb logarithm Λ_0 represents an efficient way to include the contribution from all impact parameters, without needing any special treatment of strong collisions. A conceptual problem with the perturbative derivation is that it *appears* to ignore all collisions with impact parameter less than $\rho_{\min}$. In fact, an overestimation of the contributions from small impact parameters $\rho > \rho_{\min}$ almost exactly makes up for the missing collisions with $\rho < \rho_{\min}$, as demonstrated graphically in Fig. 1. The two areas differ by a relative error which is equal to that between Λ_0 and Λ_1, less than 0.5% for $\rho_{\text{c}} = 0$ and $\Lambda_0 > 2$.

When $\rho_{\text{c}} > 0$, the perturbative treatment would replace $\rho_{\min}$ by ρ_{c} in the Coulomb logarithm, but from Eq. (7) we should replace $\rho_{\min}$ by $(\rho_{\min}^2 + \rho_{\text{c}}^2)^{1/2}$. However, it is confusing to think of this process as "replacing $\rho_{\min}$", because $\rho_{\min}$ has a specific definition, Eq. (2). Instead, we recommend keeping the roles of $\rho_{\min}$ and ρ_{c} separate, and using the modified Coulomb logarithm Λ_1.

We now calculate the total friction force on an ion in a warm electron plasma by integrating Eq. (7) over the 3D electron velocity distribution $f(\mathbf{v}_{\text{e}})$:

$$\mathbf{F}_{\parallel} = -\frac{4\pi n_{\text{e}}k^2}{m_{\text{e}}}\int_{-\infty}^{\infty}\Lambda(\mathbf{v}_{\text{rel}})\frac{\mathbf{v}_{\text{rel}}}{|\mathbf{v}_{\text{rel}}|^3}f(\mathbf{v}_{\text{e}})\mathrm{d}^3\mathbf{v}_{\text{e}}. \tag{8}$$
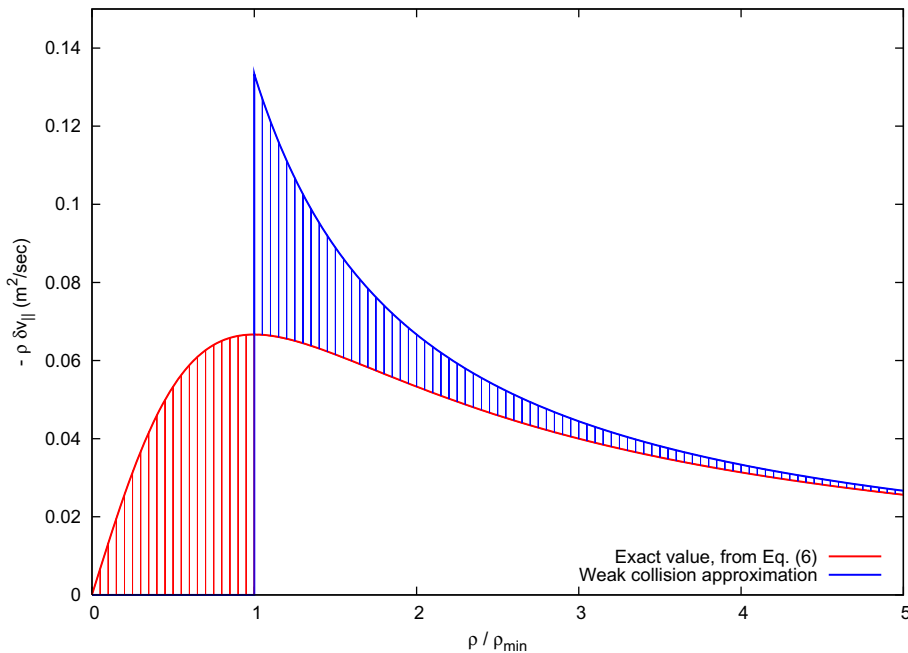

Fig. 1. Exact calculation of the friction force over impact parameter compared to the weak approximation which results in the Coulomb logarithm.

Here Λ can be either of the Coulomb logs given in Eq. (1) or (7) depending on the desired accuracy. The velocity distribution is usually assumed to be Gaussian, with different RMS values in each dimension, as given by Eq. (A.2) below. Eq. (8) must generally be evaluated numerically, as is done for example in the BETACOOL code [27].

1.2. Distinction between the friction force and electron cooling

It is important to make a distinction between simulations of the friction force on individual ions, which is the subject of the present work, and electron cooling simulations, which combine simplified models of the friction force with a variety of competing effects to study equilibration of the ion beam phase space over many turns around the storage ring or collider. The BETACOOL code [27] is one tool that can be used to estimate cooling rates over many turns. First principles simulation of the dynamical friction on individual ions provides improved physical understanding and can be used to improve the friction force models in a code like BETACOOL (see e.g. [15]).

In passing through the electron cooling section, the velocity kick on an ion can be separated into a diffusive component plus a dynamical friction component (both to be discussed in Section 6). After a single pass the diffusive kick can equal or even exceed the dynamical friction kick. Because the friction force accumulates linearly in time, while diffusive effects accumulate as the square root of the interaction time, the effects of friction will dominate over diffusion during the roughly 100 million passes through the cooling section (assuming a characteristic cooling time of 30 min). In fact, ions execute betatron (transverse) and synchrotron (longitudinal) oscillations as they travel the circumference of the RHIC collider ring, returning to the electron cooling section each time with a different phase in each dimension and, hence, different velocities with respect to the co-propagating electron beam. These details of the ion dynamics do not change the conclusion that friction will dominate diffusion over 100 million turns. What happens in BETACOOL is that the friction force, which is a function of the velocity components for a single ion, is dynamically averaged for the betatron and synchrotron phases of individual ions, and the effective cooling rate for an ion beam then depends also on an average over the (evolving) ion velocity distribution. In the VORPAL simulations presented here, we partially suppress the diffusive dynamics of ions making a single pass through the cooling section, in order to more accurately extract the friction force.

Similar considerations apply to our calculation of ρ_c. The statistical arguments presented in Appendix A show that very small impact parameters cannot be adequately sampled in a finite time, for a finite electron density, so the Coulomb logarithm Λ_1 of Eq. (7) should be used, which gives a reduction in the friction force compared to that obtained using the standard Coulomb logarithm Λ_0. It is possible that, over millions of turns, these small impact parameters are appropriately sampled and the full friction force is recovered on average. However, the ion oscillations discussed in the previous paragraph, combined with a variety of nonlinear forces, and sources of random noise like intra-beam scattering, may be sufficient to prevent small impact parameter collisions on subsequent turns from accumulating in a coherent manner. This remains an open question, to be addressed in future work.

1.3. Organization of the paper

The remainder of this paper is organized as follows: Section 2 contains a description of the physical problem, and in Sections 3–5 we give details on two numerical algorithms to solve the problem, and discuss parallelization efficiency. In Section 6 we give the parameters for the RHIC II cooler, and show that numerical models successfully simulate the diffusion in this device with zero fields. We also discuss the effect of the smallest impact parameter that can be resolved, ρ_c. In Section 7 we consider finite-time effects that arise because collisions between electrons and ions do not occur over an infinite time interval, as is often assumed by the theory. We also consider the closely related problem of how the simulation box size affects the maximum impact parameter. In Section 8 we calculate numerically how the friction changes when an external undulator magnet is present, with conclusions found in Section 9. Appendix A calculates the statistical limitation on the cutoff impact parameter ρ_c due to finite time effects, and Appendices B and C details on the binary Coulomb collision (BCC) and Hermite algorithms.

2. Problem description

Here we work in the beam-frame, where the motion of all particles is by assumption non-relativistic. We consider the interaction of a large number of electrons (N_e) with a small number of ions (N_{ion}). We assume the ion density is low, and neglect ion-ion interactions. We also neglect electron–electron interactions, although we retain the ability to "turn on" this effect in VORPAL by interaction through electrostatic PIC. By neglecting these interactions we do not have to calculate the force between every particle pair, and for N_{ion} fixed the computation time scales linearly with N_e rather than quadratically.

It is convenient to represent the positions of all particles by a single set of position vectors $\mathbf{x}_i$. The ions are represented by indices $i = 0, 1, \ldots, N_{ion} - 1$ while the electrons are $i = N_{ion}, N_{ion} + 1, \ldots, N_{ion} + N_e - 1$. We introduce a characteristic function χ_i that picks out which type of particle we have

$$\chi_i \equiv \begin{cases} 1 & \text{if } i < N_{ion}, \\ 0 & \text{if } i \geqslant N_{ion}. \end{cases}$$

We also want the ability to have more than two species of particles in our model. To do this we just modify the characteristic function, a particle species interacts with all others that differ in characteristic function value.

Let the mass of the electron and ion species be m_e and m_{ion} with charge $-e$ and Ze. The equations of motion for the system of $N_e + N_{ion}$ particles is given by the sum of the Lorentz force and Coulomb force due to particle interaction:

$$m_i \ddot{\mathbf{x}}_i = q_i(\mathbf{E} + \mathbf{v}_i \times \mathbf{B}) - \sum_j^{\chi_j \neq \chi_i} \mathbf{F}(\mathbf{x}_{ij}), \tag{9}$$

where the fields $\mathbf{E}$ and $\mathbf{B}$ are specified external fields, and

$$\mathbf{x}_{ij} = \mathbf{x}_i - \mathbf{x}_j, \tag{10}$$

$$\mathbf{F}(\mathbf{x}) = \frac{k\mathbf{x}}{|\mathbf{x}|^3} \quad \text{and} \quad k = \frac{Ze^2}{4\pi\epsilon_0}. \tag{11}$$

Note that some authors define $\mathbf{x}_{ij} = \mathbf{x}_j - \mathbf{x}_i$, which flips the sign of the sum in Eq. (9). The form of k assumes a collision between an ion of charge Ze and an electron of charge $-e$. The Coulomb force between such opposite-charge particles is attractive ($k > 0$), which corresponds to the gravitational force between astrophysical objects. In the general case we can have collisions between like-charge particles, which will give $k < 0$. We need to be sure our algorithm can handle this case.

Astrophysicists often introduce a "softening parameter" as a cutoff for the magnitude of the force. If the charge is spread uniformly in a sphere of radius r_c, we would use

$$\mathbf{F}(\mathbf{x}) = \frac{k\mathbf{x}}{(|\mathbf{x}|^2 + r_c^2)^{3/2}}. \tag{12}$$

The binary Coulomb collision algorithm described below uses an exact 2-body solver, in which case we must have $r_c = 0$. In the Hermite algorithm, the softening parameter can be used to prevent inaccuracies from very close collisions, as well as artificially limiting the impact parameter (to be discussed in the next section).

3. The Hermite algorithm

The Hermite algorithm has been adapted from one used by astrophysicists to solve n-body problems [22]. We have modified the algorithm to handle an external magnetic field, but this field must be constant in space and time. This algorithm has been used in the case of a constant solenoidal field to investigate "magnetized" cooling [6,14,15]. The Hermite algorithm originates from the idea that by taking a total derivative with respect to time of our equations of motion, we obtain an exact formula for the derivative of acceleration, called the *jerk*, $\mathbf{J}_i = \dot{\mathbf{a}}_i$. We can calculate the acceleration and jerk of the ith particle as

$$m_i \mathbf{a}_i = q_i(\mathbf{E} + \mathbf{v}_i \times \mathbf{B}) - \sum_j^{\chi_j \neq \chi_i} \mathbf{F}(\mathbf{x}_{ij}), \tag{13}$$

$$m_i \mathbf{J}_i = q_i \mathbf{a}_i \times \mathbf{B} - \sum_j^{\chi_j \neq \chi_i} \mathbf{G}(\mathbf{x}_{ij}, \mathbf{v}_{ij}), \tag{14}$$

where $\mathbf{x}_{ij} = \mathbf{x}_i - \mathbf{x}_j$, $\mathbf{v}_{ij} = \mathbf{v}_i - \mathbf{v}_j$, and G is the total time derivative of F,

$$G(\mathbf{x}, \mathbf{v}) = \dot{\mathbf{F}}(\mathbf{x}) = \frac{k\mathbf{v}}{(|\mathbf{x}|^2 + r_c^2)^{3/2}} - \frac{3k(\mathbf{v} \cdot \mathbf{x})\mathbf{x}}{(|\mathbf{x}|^2 + r_c^2)^{5/2}}. \tag{15}$$

The Hermite algorithm is a predictor–corrector method, with the predictor given by:

$$\mathbf{x}_i^p = \mathbf{x}_i + h\mathbf{v}_i + \frac{h^2}{2}\mathbf{a}_i + \frac{h^3}{6}\mathbf{J}_i, \tag{16}$$

$$\mathbf{v}_i^p = \mathbf{v}_i + h\mathbf{a}_i + \frac{h^2}{2}\mathbf{J}_i, \tag{17}$$

where h is the time step (at this point assumed to be the same for all particles).

We now write Taylor series for the positions, velocities, and all derivatives up to jerk. Note that the subscript "0" refers to a quantity at the start of a time step, and "1" the end of a time step.

$$\mathbf{x}_{1,i} = \mathbf{x}_{0,i} + \mathbf{v}_{0,i}h + \frac{1}{2}\mathbf{a}_{0,i}h^2 + \frac{1}{6}\mathbf{J}_{0,i}h^3 + \frac{1}{24}\mathbf{S}_{0,i}h^4 + \frac{1}{120}\mathbf{C}_{0,i}h^5, \tag{18}$$

$$\mathbf{v}_{1,i} = \mathbf{v}_{0,i} + \mathbf{a}_{0,i}h + \frac{1}{2}\mathbf{J}_{0,i}h^2 + \frac{1}{6}\mathbf{S}_{0,i}h^3 + \frac{1}{24}\mathbf{C}_{0,i}h^4, \tag{19}$$

$$\mathbf{a}_{1,i} = \mathbf{a}_{0,i} + \mathbf{J}_{0,i}h + \frac{1}{2}\mathbf{S}_{0,i}h^2 + \frac{1}{6}\mathbf{C}_{0,i}h^3, \tag{20}$$

$$\mathbf{J}_{1,i} = \mathbf{J}_{0,i} + \mathbf{S}_{0,i}h + \frac{1}{2}\mathbf{C}_{0,i}h^2, \tag{21}$$

where $\mathbf{S}_{0,i}$ and $\mathbf{C}_{0,i}$ are the second and third time derivatives of the acceleration at time $t = 0$, called the **snap** and **crackle**. We are approximating the solution using an interpolating polynomial in h with derivatives through order five specified at $t = 0$. This process in general is known as Hermite interpolation, from which this algorithm derives its name. We can now solve Eqs. (20) and (21) for $\mathbf{S}_{0,i}$ and $\mathbf{C}_{0,i}$ in terms of the acceleration and jerk, giving

$$\mathbf{S}_{0,i} = -2\frac{3(\mathbf{a}_{0,i} - \mathbf{a}_{1,i}) + h(2\mathbf{J}_{0,i} + \mathbf{J}_{1,i})}{h^2},\tag{22}$$

$$\mathbf{C}_{0,i} = 6\frac{2(\mathbf{a}_{0,i} - \mathbf{a}_{1,i}) + h(\mathbf{J}_{0,i} + \mathbf{J}_{1,i})}{h^3}.\tag{23}$$

The corrector then applies these quantities in the Taylor series introduced above,

$$\mathbf{x}_i(t + h) = \mathbf{x}_i^p + \frac{h^4}{24}\mathbf{S}_{0,i} + \frac{h^5}{120}\mathbf{C}_{0,i},\tag{24}$$

$$\mathbf{v}_i(t + h) = \mathbf{v}_i^p + \frac{h^3}{6}\mathbf{S}_{0,i} + \frac{h^4}{24}\mathbf{C}_{0,i}.\tag{25}$$

This algorithm is self-starting, and proceeds by the following steps:

1. Calculate the initial acceleration $\mathbf{a}_{0,i}$ and jerk $\mathbf{J}_{0,i}$ using Eqs. (13) and (14). This step is only executed once, for the first time step.
2. Calculate new position and velocities using the predictors Eqs. (16) and (17).
3. Calculate the new acceleration $\mathbf{a}_{1,i}$ and jerk $\mathbf{J}_{1,i}$ using Eqs. (13) and (14) on the predicted positions and velocities.
4. Calculate the snap and crackle using Eqs. (22) and (23).
5. Advance to the next time step by using the correctors Eqs. (24) and (25).
6. Determine h_i, the next time step for particle i (different for each particle).
7. Set all $\mathbf{a}_{0,i} = \mathbf{a}_{1,i}$, $\mathbf{J}_{0,i} = \mathbf{J}_{1,i}$, and return to Step 2.

Note that the predictors calculate $\mathbf{x}_i$ up to $O(h^4)$ and $\mathbf{v}_i$ up to $O(h^3)$. When there are no external fields present, the acceleration and jerk of Eqs. (13) and (14) have errors $O(h^4)$ and $O(h^3)$, respectively, so that the snap and crackle in Eqs. (22) and (23) are determined up to $O(h^2)$ and $O(h)$. The corrector thus has single step error $O(h^5)$, and the method overall is 4th-order. However when external fields are present, the acceleration Eq. (13) depends on the velocity, not just the positions of the particles, and so it is determined up to $O(h^3)$. This means that the crackle error is $O(1)$, which breaks the 4th-order accuracy of the corrector. If implemented as stated, the new algorithm with $B \neq 0$ will be 3rd-order.

Breaking of 4th-order accuracy is due to the linear term $q_i\mathbf{v}_i \times \mathbf{B}$, and it can be restored by the following technique: First, we divide $\mathbf{a}_i$, $\mathbf{J}_i$, $\mathbf{S}_i$ and $\mathbf{C}_i$ into two pieces, the first due to the Lorentz force, and the second due to particle interaction. The predictor and corrector formulas now have twice as many terms to be added. As shown in Appendix B, 4th-order accuracy of the scheme can be retained with two modifications of the algorithm:

- In Step 3: Calculate the acceleration and jerk with the fields evaluated at the predicted values of position and velocity.
- In Step 5: For the part of the solution corresponding to the fields only, change the coefficient in Eq. (24) from 1/120 to 1/60, and in Eq. (25) from 1/24 to 5/72.

To resolve close collisions, the time step must be reduced. It is much more efficient if we only reduce the time step for strongly interacting particles. To do so we introduce a hierarchy of time steps

$$h(n) = h\left(\frac{1}{2}\right)^{n-1}; \quad n = 1, 2, \ldots 15,$$

where h is the base time step. We have found that 15 time step levels is generally sufficient. The algorithm proceeds by updating the particles with the smallest current time.

To determine the next time step for particle i, Aarseth [1] suggests

$$h_i = \left(\eta \frac{|\mathbf{a}_{1,i}||\mathbf{S}_{1,i}| + |\mathbf{J}_{1,i}|^2}{|\mathbf{J}_{1,i}||\mathbf{C}_{1,i}| + |\mathbf{S}_{1,i}|^2}\right)^{1/2},\tag{26}$$

where η is a dimensionless constant. Aarseth has found that $\eta = 0.03$ gives energy conservation to one part in 10^4 *in the absence of close encounters* [1]. Numerical experiments with two particles and $r_c = 0$ have found that Eq. (26) does not always reduce the stepsize fast enough during strong collisions.

A formula for the next time step for particle i that works even when $r_c = 0$ is

$$h_i = \frac{1}{C} \min_j^{\chi_j \neq \chi_i} \frac{|\mathbf{x}_{ij}|}{|\mathbf{v}_{ij}|},\tag{27}$$

where C is the minimum number of time steps before two particles can coincide. We have found that a choice of $C = 10$ works well. For the general n-body problem for one time step over all particles, Eq. (27) requires $O(N^2)$ divisions, while Eq. (26) over all particles scales as $O(N)$. However, for Eq. (27) we only recalculate the time step for each electron, and there are only a small number of ions in the minimization. In order to fully resolve all collisions, we use $r_c = 0$, with the next time step level selected using Eq. (27).

4. The binary Coulomb collision (BCC) algorithm

The idea for the BCC algorithm comes from the observation that the vast majority of electron–ion collisions are weak and easy to calculate, with only the occasional strong collision requiring more numerical effort. We can create an algorithm that solves Eq. (9) by summing exact 2-body collision solutions over each pair of interacting particles. One benefit of this technique is that it enables us to take a constant time step.

We cannot solve the 2-body problem exactly in the presence of arbitrary electric and magnetic fields, so the BCC algorithm assumes $\mathbf{B} = \mathbf{E} = \mathbf{0}$. Particle motion due to these external fields is handled using an operator splitting technique, alternately applying binary Coulomb collision and field pushes. It is not practical to use this operator splitting technique with the Hermite algorithm, because the time step for each particle depends on information from the previous time step. Hence, the insertion of a new operator that changes particle positions or velocities will break the time step calculation of the Hermite algorithm.

The BCC algorithm is defined by the following time advance formulas:

$$\mathbf{x}_i(t + h) = \mathbf{x}_i + \underbrace{h\mathbf{v}_i}_{\text{drift}} + \frac{\mu}{m_i} \sum_{j}^{\chi_j \neq \chi_i} \delta\mathbf{x}_{ij}, \tag{28}$$

$$\mathbf{v}_i(t + h) = \mathbf{v}_i + \frac{\mu}{m_i} \sum_{j}^{\chi_j \neq \chi_i} \delta\mathbf{v}_{ij}, \tag{29}$$

where $\mu = m_e m_{\text{ion}}/(m_e + m_{\text{ion}})$ is the reduced mass of the electron–ion pair. The terms $\delta\mathbf{x}_{ij}$ and $\delta\mathbf{v}_{ij}$ come from the exact solution to the two-body problem between particles i and j, and are defined by

$$\delta\mathbf{x}_{ij} = [\mathbf{e}_{ij}(h) - \mathbf{e}_{ij}(0)] - h\dot{\mathbf{e}}_{ij}(0), \tag{30}$$

$$\delta\mathbf{v}_{ij} = [\dot{\mathbf{e}}_{ij}(h) - \dot{\mathbf{e}}_{ij}(0)]. \tag{31}$$

Here $\mathbf{e}_{ij}(t)$ is the exact solution at time t of the reduced 2-body problem for the interaction of particles i and j, and $t = 0$ corresponds to the initial condition at the beginning of the time step.

$$\mu\ddot{\mathbf{e}}_{ij} = -\mathbf{F}(\mathbf{e}_{ij}) \quad \text{with initial conditions} \tag{32}$$
$$\mathbf{e}_{ij}(0) = \mathbf{x}_{ij}(0) = \mathbf{x}_i(0) - \mathbf{x}_j(0) \quad \text{and}$$
$$\dot{\mathbf{e}}_{ij}(0) = \dot{\mathbf{x}}_{ij}(0) = \dot{\mathbf{x}}_i(0) - \dot{\mathbf{x}}_j(0).$$

For a two-particle system, Eqs. (28) and (29) are one way to write the conversion formulas between motion of a single reduced particle of mass μ under a central force back to the original two-particle system. For this two-particle system, the BCC algorithm gives the exact solution, *for any time step*. For a system of more than two particles, the BCC algorithm gives an approximation to the solution. Details on solving the 2-body problem exactly can be found in Appendix B.

When $i < j$, $\delta\mathbf{x}_{ij}$ represents the correction to the motion of ion i in response to electron j. It is computationally expensive to calculate this, and we do not want to repeat this work when calculating $\delta\mathbf{x}_{ji}$, the correction to the motion of electron j in response to ion i. As a consequence of momentum conservation, $\delta\mathbf{x}_{ij} = -\delta\mathbf{x}_{ji}$ and $\delta\mathbf{v}_{ij} = -\delta\mathbf{v}_{ji}$, in practice we compute these deviations once for $i < j$ and add them to ion i and subtract them from electron j.

If we perform a Taylor expansion of $\mathbf{e}_{ij}(t)$ and $\dot{\mathbf{e}}_{ij}(t)$ around $t = 0$, and substitute back into Eqs. (30) and (31), we obtain

$$\delta\mathbf{x}_{ij} = \frac{h^2}{2}\ddot{\mathbf{e}}_{ij}(0) + \frac{h^3}{6}\dddot{\mathbf{e}}_{ij}(0) + O(h^4). \tag{33}$$

However, $\ddot{\mathbf{e}}_{ij}(0) = -\mathbf{F}(\mathbf{x}_{ij}(0))/\mu$, and $\dddot{\mathbf{e}}_{ij}(0) = -\mathbf{G}(\mathbf{x}_{ij}(0), \mathbf{v}_{ij}(0))/\mu$, where $\mathbf{G}(\mathbf{x}, \mathbf{v})$ is the exact time derivative of $\mathbf{F}$ as defined in Eq. (15). Substitution into the time advance equations Eqs. (28) and (29) gives exactly the Hermite predictor, Eqs. (16) and (17), up to order $O(h^4)$ in $\mathbf{x}_i$ and $O(h^3)$ in $\mathbf{v}_i$. This proves that when $\mathbf{E} = \mathbf{B} = \mathbf{0}$, the BCC algorithm converges to the solution to Eq. (9) as $h \to 0$, and is equivalent to the Hermite predictor as $h \to 0$. Moreover, because the single step error is $O(h^3)$, the BCC algorithm is a 2nd-order method.

This shows that the BCC algorithm will converge more slowly than the Hermite algorithm, and indeed in general n-body problems where many particles are separated by similar distances, it is inferior. In our simulations, most of the electrons are relatively far from any ion, with only the occasional close collision.

Solving the two-body problem exactly for all electron–ion pairs is computationally expensive, and for many pairs the interaction is very weak. We estimate the distance of closest approach during the next time step, assuming the two particles

travel in straight lines. If the ratio of the maximum potential energy to starting kinetic energy is less than some threshold, we use the Hermite predictor,

$$\delta \mathbf{x}_{ij} \cong -\frac{1}{\mu}\left[\frac{h^2}{2}\mathbf{F}(\mathbf{x}_{ij}) + \frac{h^3}{6}\mathbf{G}(\mathbf{x}_{ij}, \mathbf{v}_{ij})\right], \tag{34}$$

$$\delta \mathbf{v}_{ij} \cong -\frac{1}{\mu}\left[\frac{h^2}{2}\mathbf{G}(\mathbf{x}_{ij}, \mathbf{v}_{ij})\right], \quad \text{with } r_c = 0. \tag{35}$$

In practice 70–90% of all collisions may be calculated using this fast technique.

5. Operator splitting and code parallelization

In the BCC algorithm, the interaction of particles with fields is handled using a standard Boris push algorithm [5], which proceeds using the following symmetric steps:

1. Drift($h/2$).
2. E-kick($h/2$).
3. B-kick(h).
4. E-kick($h/2$).
5. Drift($h/2$).

The B-kick step is a simple 2nd-order scheme which exactly conserves particle kinetic energy. The drifts only modify particle locations, while the E and B kicks only modify particle velocity.

Since the Boris push and BCC algorithms are both 2nd-order, one can simply apply them alternately. However such a scheme is only 1st-order overall. One way to retain 2nd-order accuracy is to preserve the symmetry of the algorithm, and since the BCC algorithm takes the greatest amount of time, it is best to place it in the middle of a symmetric scheme:

1. E-kick($h/2$).
2. B-kick($h/2$).
3. BCC(h).
4. B-kick($h/2$).
5. E-kick($h/2$).

Note that in Step 3, the BCC algorithm Eqs. (28) and (29) includes the particle drift.

Fig. 2 shows convergence rates for the Hermite algorithm compared with the BCC with symmetrized Boris push. We solve the 3-body problem in 2D in the presence of a constant magnetic field. The vertical axis shows the relative change in total energy, which is zero for the exact solution. In problem #1, the three bodies are separated by the same distance, and we see
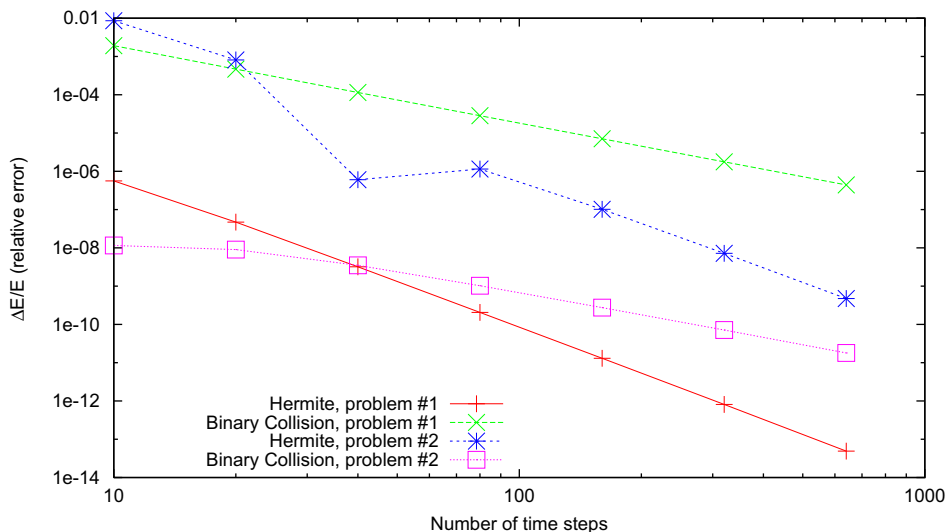

Fig. 2. Convergence rates of the Hermite and BCC algorithms for solving the 3-body problem.
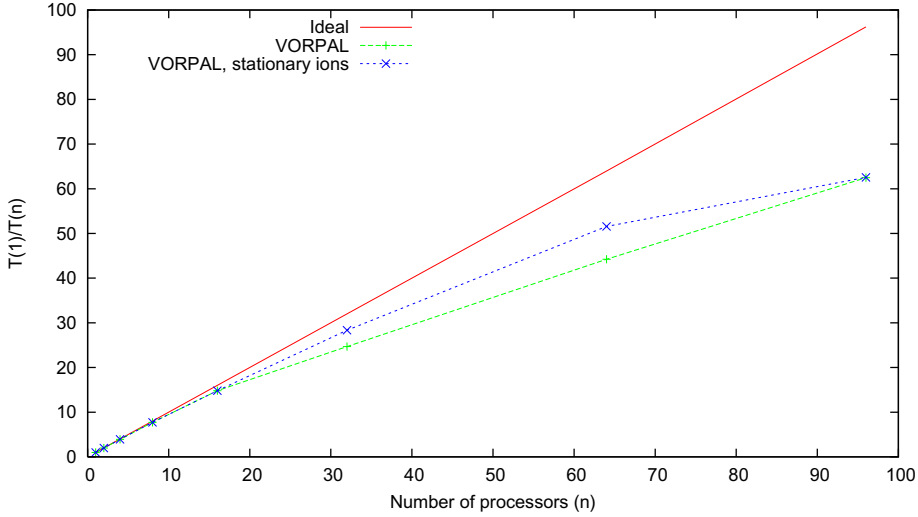
Fig. 3. Scaling of the BCC algorithm in parallel VORPAL runs. $T(n)$ is the CPU time for the same problem run on n processors.

that the Hermite algorithm always has a smaller error. In problem #2, two of the bodies are 100 times closer together compared to the third, and the accuracy of the algorithms is reversed (for this range of time steps). Fig. 2 shows that the BCC algorithm tolerates a larger time step, provided only one pair of particles is interacting strongly.

The Hermite algorithm is difficult to parallelize because of the hierarchy of time steps, and we have only run it using the serial version of VORPAL. We have found that the algorithm is more efficient if the relatively heavy gold ions are prevented from dropping down in time step, and the algorithm suffers no loss of accuracy.

The BCC algorithm parallelizes easily because of the constant time step, and pairwise interaction formula. The Boris push parallelizes trivially because it only involves one particle and the local field. At the beginning of each binary collision time step, the processors share the position and velocity of all ions. Each processor is then able to calculate the contributions $\delta\mathbf{x}_{ij}$ and $\delta\mathbf{v}_{ij}$ for collisions between any ion and any electron in its domain. At the end of the BCC update the processors share ion kicks, which are summed over each ion in the processor's domain.

Fig. 3 shows parallel timing runs for the same problem run on different numbers of processors. The cluster used has 24 dual-core, dual-processor nodes, made up of 1.8 GHz Opteron processors with 4 GB of memory, interconnected using GB ethernet. Each run uses 8 equally-separated ions, and for this reason parallelization is essentially perfect (doubling of speed with each doubling of the number of processors) up to eight processors. Beyond this some domains contain no ions, and these finish more quickly due to a higher percentage of weak collisions. The total time in this case is controlled by the processors which contain ions. Here we are using the automatic domain decomposition in VORPAL, which results in equal size domains. We can improve the parallelization by moving into the frame of reference of the ions and adjusting the domain sizes so that the domains containing ions are smaller. The third curve in Fig. 3 shows the effect of this first change.

6. Diffusive effects and the resolution of small impact parameters

Analogous to the frictional force, Eq. (8), the momentum diffusion tensor can be calculated as [8,10]

$$d_{\alpha\beta} = 4\pi n_e k^2 \int \Lambda_0 \frac{|\mathbf{v}_{rel}|^2 \delta_{\alpha\beta} - v_\alpha v_\beta}{|\mathbf{v}_{rel}|^3} f(\mathbf{v}_e) d^3 v_e. \tag{36}$$

Note that ρ_{min} in the Coulomb logarithm Λ_0 varies with the relative speed of the ion and electron, but it is often taken as a constant by using the average value of $|\mathbf{v}|^2$. In this case the Coulomb logarithm is often taken outside the integrals in Eqs. (8) and (36). It is more correct to keep Λ_0 inside the integral, but any differences are small in the limit that $\Lambda_0 \gg 1$.

We have simulated the friction force using the parameters shown in Table 1, which are relevant to the proposed RHIC electron cooler. We simulate a small portion of the beam, a cube approximately $L \approx 1$ mm on a side. The electron density in this domain is assumed constant, and we impose periodic boundary conditions along all three axes x, y and z. These simulations typically use eight equidistant ions.

The run time for this algorithm scales as $N_e N_{ion}$, and since we are free to choose the number of ions, this suggests we should use as few as possible. For one ion we get a single number for the friction force, the advantage of using eight ions is that we get eight estimates of the friction, and the standard deviation can be used to estimate the error, as shown in Fig. 4.

The algorithms we use are specialized to the free-space inverse square law of the Coulomb force, so we cannot use an Ewald potential or other modified force laws to impose periodicity on the electrostatic fields of the charged particles. Hence,

Table 1
RHIC cooling section parameters (as of 2006)

Parameter	Frame	Value
Electron density, n_e	Beam	9.50×10^{13} e$^-$/m^3
RMS e^- x, y-velocity, Δ_x, Δ_y	Beam	2.8×10^5 m/s
RMS e^- z-velocity, Δ_z	Beam	9.0×10^4 m/s
Interaction time, τ	Beam	2.47×10^{-9} s
90° collision impact parameter, ρ_{min}	Beam	2.2×10^{-7} m
Mean Coulomb log value, Λ_0	Beam	8.2
Relativistic γ	Lab	108
Relativistic $\beta = v/c$	Lab	0.99957
Undulator length	Lab	80 m
Undulator strength	Lab	10 G or 1.0×10^{-3} Tesla
Undulator wavelength, λ	Lab	8 cm
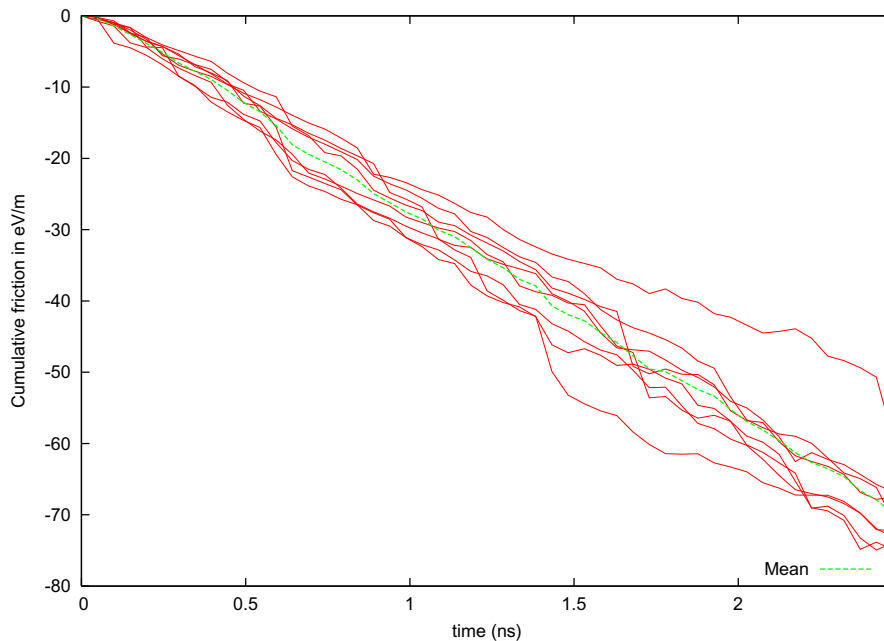
Fig. 4. Cumulative longitudinal friction in a VORPAL simulation for eight gold ions. The vertical scale is proportional to the velocity change.

we use the following numerical technique to eliminate bulk electric forces on ions that are not in the precise center of the simulation domain. The position of each electron, relative to an ion, is cyclically shifted before the force is evaluated in Eq. (11) so that ion sees an equal number of electrons on each side and is, effectively, in the center of a cubic distribution of electrons.

For example, if any coordinate component $x_{ij} > L/2$, then the value $x_{ij} - L$ is used in Eq. (11) instead of x_{ij}. On the other hand, if $x_{ij} < -L/2$, then $x_{ij} + L$ is used. Tests have shown that this simple and numerically efficient technique yields the same simulated friction force as is obtained when working in the rest frame of a single ion which remains in the center of a cubic domain while electrons stream past. Additional evidence can be found in the plots of friction versus the box size L, as in Fig. 7. If there was some error associated with the cyclic shifting technique, one would expect it to be greater the smaller the box size, yet such an effect is not seen.

The diffusive kicks on the ion cause it to perform a random walk, with the resulting RMS velocity spread increasing as $\sqrt{t}$. Fig. 5 shows a comparison between the diffusion predicted by Eq. (36) and VORPAL simulation results. For the finite interaction time of the RHIC cooling section, the friction force is small compared to the diffusive velocity kicks.

For the electron density of the RHIC cooling section, there are of order 50,000 electrons in a domain $L = 0.8$ mm on a side. Passage through the 80 m RHIC cooler takes about 2.5 ns (in the beam-frame), and diffusion dominates over friction for this short time interval. To obtain a statistically significant friction force, we must do hundreds of runs and average the resulting ion velocity changes. Alternatively, we can divide both the charge and mass of each electron by an integer N_m, and use N_m times more electrons. In this manner we can do a single large VORPAL run and take advantage of the parallelization; otherwise, one would have to do many small simulations using a task farming approach, which is much less convenient. Note,
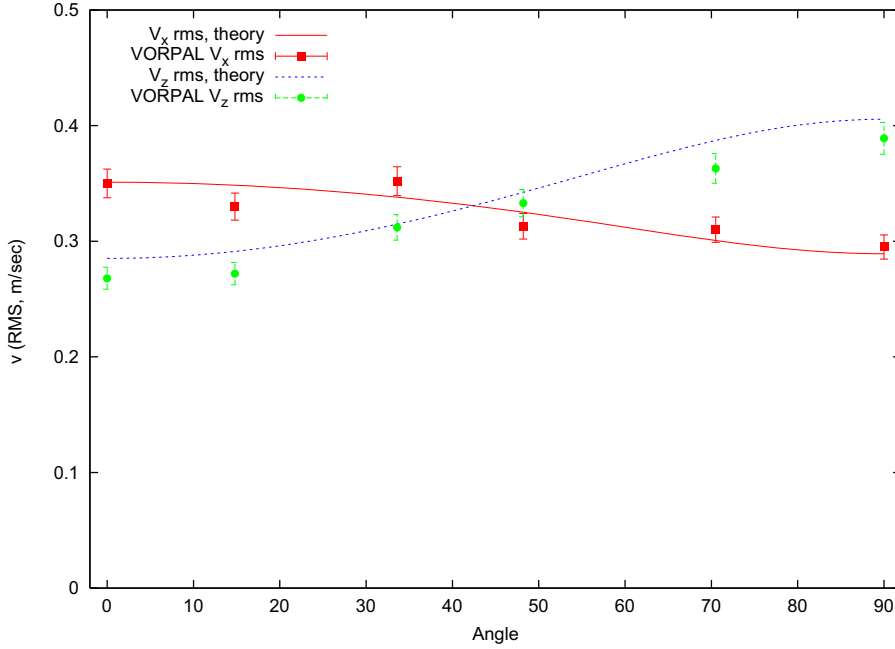
Fig. 5. The diffusion predicted by Eq. (36) compared with that seen in VORPAL runs ($B = 0$). The diffusion is measured by the RMS velocity of the gold ions.

however, that according to the analysis in Appendix A, averaging many runs, or splitting each electron into N_m particles, reduces the cutoff impact parameter resolved by the simulation ρ_c, which tends to increase the friction force.

To reduce the diffusion in numerical simulations, we note that the frictional force in Eq. (8) is independent of the sign of the charges. In VORPAL, we replace half the electrons by positrons with identical initial positions and velocities. The field seen by the positrons is set to the negative of the field seen by the electrons, so that in the absence of ions, the electrons and positrons would move identically. Any diffusive kick given to an ion by an electron will be approximately canceled by a negative kick from its paired positron, greatly reducing the diffusion. This trick can be used whenever Eq. (8) is valid, which requires that the Coulomb logarithm $\Lambda_0 \gg 1$ (see Appendix A).

Fig. 6 shows the friction force of Eq. (8) calculated using Λ_1, with the x-axis being the upper limit of integration in ρ. All parameters used are for the RHIC cooler of Table 1. The curve shows that 8.3% of the total friction force is due to impact parameters less than $\rho_{\min}$. In Appendix A, we show how to calculate the cutoff impact parameter that can be resolved in finite time, ρ_c. In the numerical simulations, $\rho_c \approx 2.4\rho_{\min} = 5.3 \times 10^{-7}$ m, so Fig. 6 suggests that physical friction force as simulated by VORPAL will be 17% lower than predicted by the standard Coulomb logarithm.

7. Finite time and box size effects

Earlier we saw that a careful treatment of small impact parameter collisions gave the modified Coulomb logarithm Λ_1 in Eq. (7). Another effect we now wish to take into account is that all collisions occur during a finite time interval. This has relatively little effect on small impact parameter collisions, but becomes significant for large impact parameter collisions. We will now see that these finite collision time effects result in an additional modification to the Coulomb logarithm.

In the standard perturbative derivation of the friction force [8], the force due to each electron is integrated over an infinitely long trajectory. However, the integrals can be done exactly for finite length trajectories (i.e. for a finite time), if all collisions are assumed to be symmetric. A length scale which emerges as significant is half the length of the collision trajectory, $d = |\mathbf{v}_{\text{rel}}| \, \tau/2$. For finite-time, symmetric collisions with $d \gg \rho_{\min}$, the friction force obtained is Eq. (7), with the Coulomb logarithm Λ replaced by

$$\Lambda_2(\rho_{\max}, \rho_{\min}, \rho_c, d) = \frac{1}{2} \ln \left[\left(\frac{\rho_{\max}^2 + \rho_{\min}^2}{\rho_{\min}^2 + \rho_c^2} \right) \left(\frac{\rho_c^2 + d^2}{\rho_{\max}^2 + d^2} \right) \right]. \tag{37}$$

Various limiting cases reduce to previous results. For example, if $d \gg \rho_{\max}$, we recover Λ_1 of Eq. (7), and if we also have $\rho_{\max} \gg \rho_{\min}$ and $\rho_c = 0$ we recover Λ_0 of Eq. (1). If $\rho_{\max} \gg d$ and $\rho_c = 0$, then Λ_2 reduces to Λ_0 where $\rho_{\max}$ is replaced by d, so that the maximum impact parameter is controlled by the interaction time τ.

Since the numerical model approaches the collisions from first principles, one might assume that it is free of artificial cutoffs in impact parameter. However, this is not the case. There is an upper limit imposed by the size of the domain, L. The
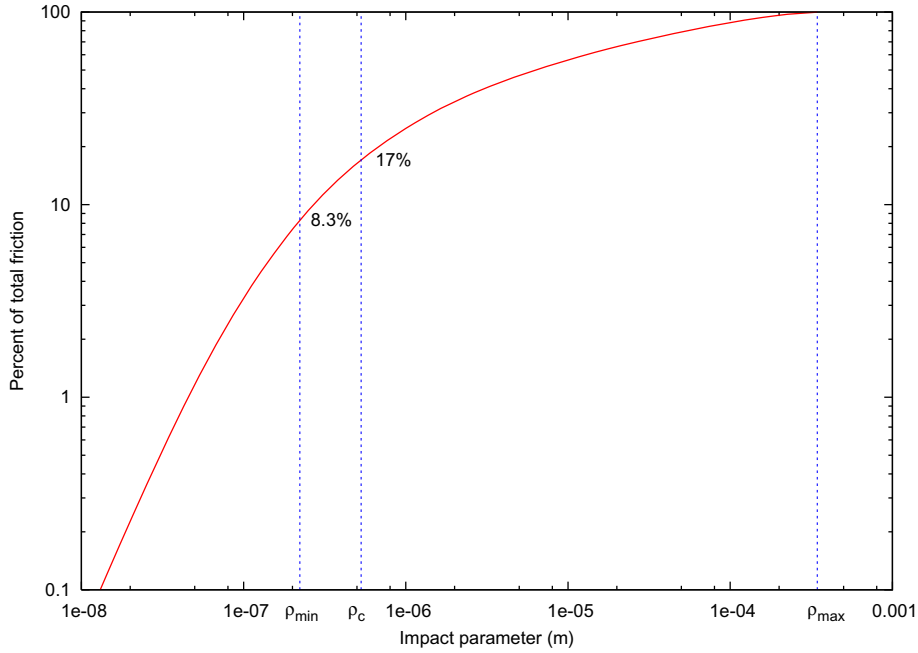
Fig. 6. Cumulative friction by impact parameter. If there are no collisions with impact perimeter less than ρ_c, the dynamical friction will be reduced by 17%.

length of an electron trajectory can be no longer than $\sqrt{3}L$, and numerically for the electron parameters in Table 1 we find the mean trajectory length is $0.86L$. This is simply a geometric property of an electron placed randomly in a box, with a random velocity. In the Coulomb logarithm Λ_2 of Eq. (37), we should use half this trajectory length for $\rho_{max} = 0.43L$ and $d = \min\{|\mathbf{v}_{rel}|\ \tau/2, \rho_{max}\}$. In the physical RHIC collider, the maximum impact parameter is limited by the size of the beam, as well as the finite interaction time, and the beam is large enough that the latter determines $\rho_{max} = |\mathbf{v}_{rel}|\ \tau/2$.

Fig. 7 shows a comparison between friction predicted by Eq. (8) and VORPAL simulations using various box sizes. Here the theoretical curve uses the Coulomb logarithm Eq. (37). In calculating σ_{finite}, it is important to replace the trajectory length $\langle v_{rel}\rangle\tau$ in Eq. (A.5) by $0.86\ L$ when the latter is smaller, so that σ_{finite} depends on L.

In Fig. 8 we compare the longitudinal and transverse friction for an ion moving at velocity 3.0×10^5 m/sec. The angle (x-axis) refers to the angle of the gold ion's velocity, where $0°$ is longitudinal, and $90°$ is transverse.

8. Effects of adding an undulator magnet

A helical undulating field in the lab frame with wavelength λ in cylindrical coordinates is given by [18],

$$B_{lab}(r, \theta, z) = 2B_0\left[I_1'(\ell r)\cos(\theta - \ell z)\hat{r} + I_1(\ell r)\sin(\theta - \ell z)\left(\hat{z} - \frac{\hat{\theta}}{\ell r}\right)\right],$$

where $\ell = 2\pi/\lambda$ and I_1 is a modified Bessel function. When Lorentz transformed to the beam-frame, assuming $r \ll \lambda$, to leading order we have only time-dependent electric and magnetic fields, which can be written in Cartesian coordinates as:

$$E_{beam}(x, y, z) = E_0[-(\sin\Omega t)\hat{x} + (\cos\Omega t)\hat{y}],$$
$$B_{beam}(x, y, z) = \gamma B_0[(\cos\Omega t)\hat{x} + (\sin\Omega t)\hat{y}],$$

where $E_0 = \gamma\beta c B_0$ and $\Omega = \gamma\beta c\ell = 2\pi\gamma\beta c/\lambda$.

The undulator field causes the electrons to undergo transverse oscillations in the beam-frame [19] of magnitude $r_0 = e\lambda^2 B_0/(4\pi^2 m_e \gamma\beta c) = 8.8 \times 10^{-7}$ m (for $B_0 = 1.0 \times 10^{-3}$ Tesla). The Coulomb collisions with impact parameter less than r_0 will no longer occur, and if the relative velocities of the electrons are not altered significantly enough to affect the velocity term in Eq. (8), the friction should be reduced by a factor of

$$f = \frac{\Lambda_2(\rho_{max}, \rho_{min}, \rho_c, d)}{\Lambda_2(\rho_{max}, \rho_{min}, \kappa r_0, d)} \cong \frac{\ln(\rho_{max}/\rho_c)}{\ln(\rho_{max}/\kappa r_0)}, \tag{38}$$

where $\kappa \geqslant 1$ is a constant. The value of $\kappa = 1$ has been suggested previously [2,3,11,16].

In Eq. (38) we use $\rho_{max} = 0.43L$, $\rho_c = 2.4\rho_{min}$ and $\kappa = 2$. This gives a factor f of 1.23 for $B_0 = 1.0 \times 10^{-3}$ Tesla and 1.77 for $B_0 = 5.0 \times 10^{-3}$ Tesla. Figs. 9 and 10 show the longitudinal and transverse friction for these two field strengths for VORPAL
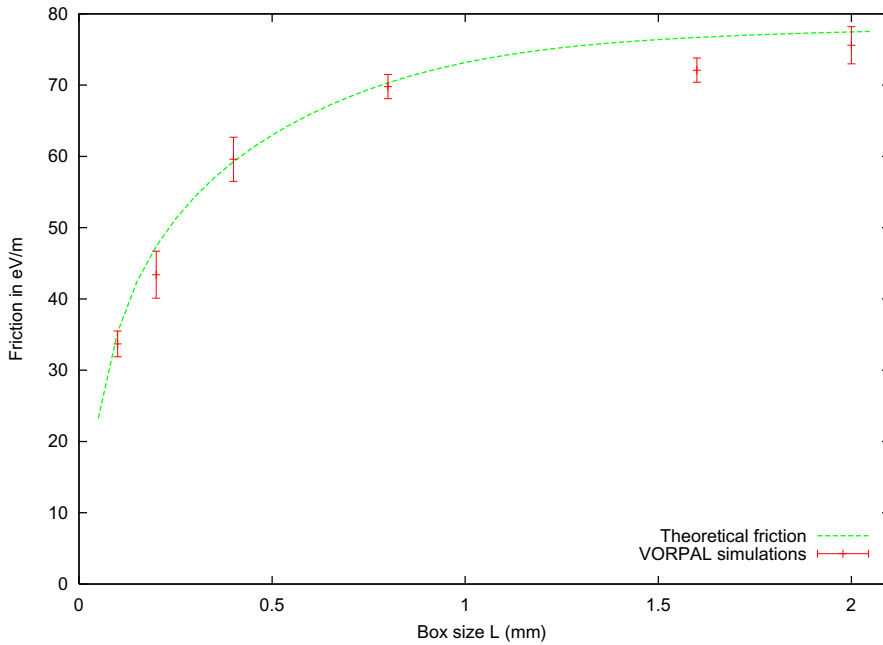
Fig. 7. The impact of the box size L on the simulated friction. For the theoretical curve, it is important to include finite-time effects on both ρ_{max} and ρ_{c}.
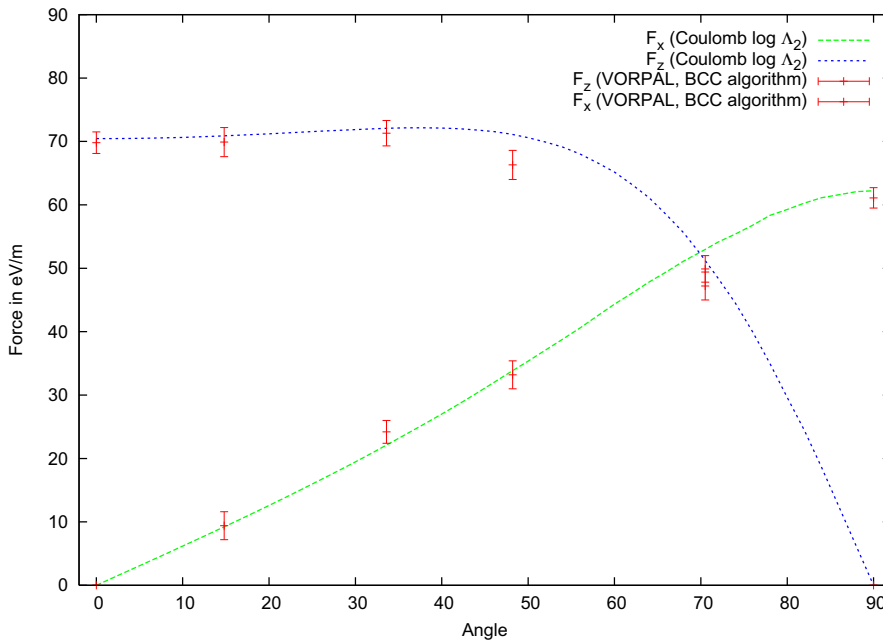

Fig. 8. A comparison of the friction from VORPAL simulations and Eq. (8) using the Coulomb logarithm Λ_2 (Eq. (37)). The external field is zero.

runs and theoretical calculations. The theoretical curves for $B = 0$ use the Coulomb logarithm Eq. (37), for $B > 0$ we simply reduce the $B = 0$ curve by the factor f. A value of $\kappa = 2$ produces a good match with the VORPAL simulations. It is reasonable to take $\kappa \geqslant 1$, but we can find no other physical argument for the value of κ, and it may differ in other parameter regimes. It has been shown with BETACOOL simulations that this reduction in the friction force, and the associated reduction in electron recombination, can be used to find an optimal undulator field strength [17]. The impact of general fields on the friction force will be explored in much more detail in a future paper.
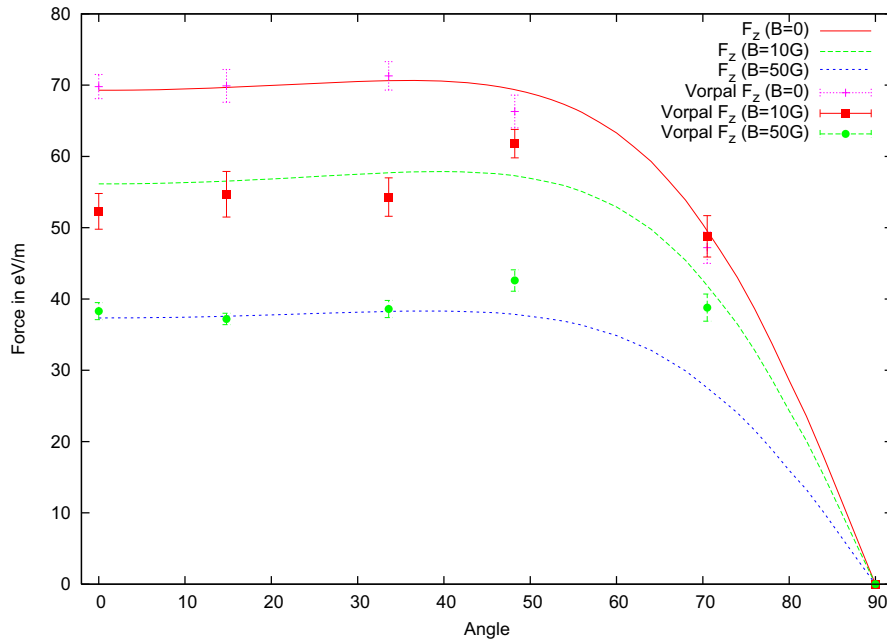
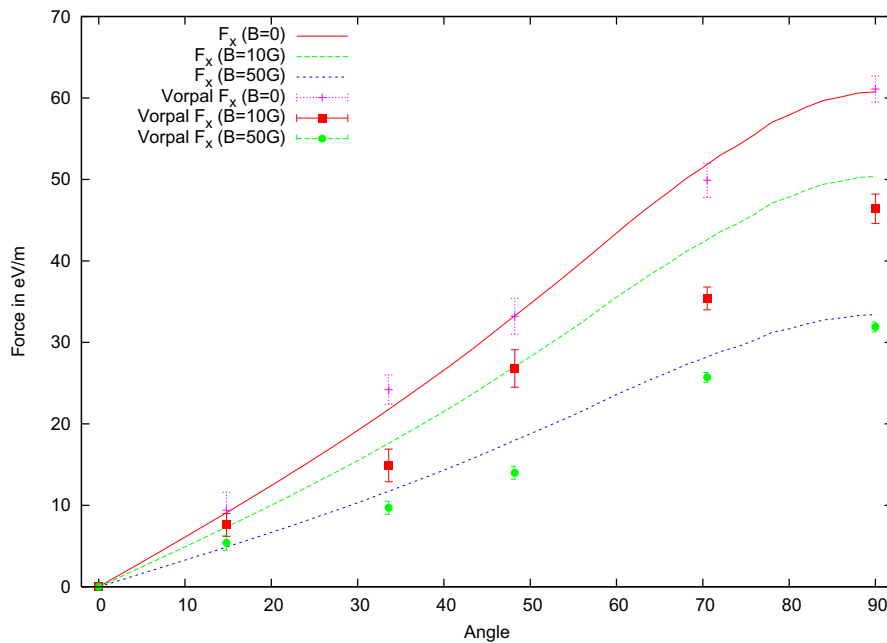Fig. 9. Longitudinal friction for $B = 0$ and with a 10 G and 50 G undulator.

Fig. 10. Transverse friction for $B = 0$ and with a 10 G and 50 G undulator.

9. Conclusions

We have presented two algorithms for simulating the dynamical friction force on ions due to a co-propagating beam of electrons. The Hermite algorithm is a 4th-order method which works in the case of a constant magnetic field. The binary Coulomb collision (BCC) algorithm is 2nd-order and can be used in the presence of rapidly varying and arbitrarily strong electric and magnetic fields. Despite the lower order of the BCC algorithm, it tolerates a much larger time step compared to the Hermite algorithm, and in general one chooses the time step according to the rate of change of any external fields.

We have considered physical parameters of the proposed RHIC cooling section. Compared to existing electron cooling facilities, these parameters are characterized by a relatively low electron density and short interaction time. One must carefully consider finite time effects to correctly interpret any simulation of the friction force in this parameter regime. We have done so by reviewing in detail the standard perturbative calculation that results in the Coulomb logarithm, with carefully separation of the roles of ρ_{min}, ρ_c and ρ_{max}. In particular, we have shown that finite time effects can strongly constrain ρ_{max} from above and ρ_c from below, and naive application of the standard Coulomb logarithm can significantly over-estimate the magnitude of the friction force. We have shown that theoretical predictions closely match VORPAL simulation results when we use a modified Coulomb logarithm Λ_2, Eq. (37) in Eq. (8).

We have simulated the proposed RHIC cooling section, including a 10 G, 8 cm wavelength helical undulator. We have compared the friction obtained with the undulator to the friction when no fields are present. Theoretical estimates that friction will be reduced by the factor given in Eq. (38) have been confirmed by the BCC algorithm. In short, the effective value of ρ_c is κ times the usual oscillation amplitude for electrons in an undulator magnet, where $\kappa \geqslant 1$ is a constant depending on the simulation parameters. A value of $\kappa = 2$ works well for the RHIC parameters.

Acknowledgments

Appendix A. Statistical limitations on small impact parameters

For a spatially uniform electron density n_e, the typical inter-particle separation is $a = (4\pi n_e/3)^{-1/3}$, sometimes called the Wigner-Seitz radius [29,30]. We consider the probability that the distance between a single ion and any number of electrons will become less than ρ in a time τ, for values of $\rho \ll a$. We assume unperturbed ion motion with velocity $\mathbf{v}_{ion} = v_{ion,x}\hat{x} + v_{ion,z}\hat{z}$, and consider times short compared to a plasma period, $\omega_{pe}\tau < 2\pi$, so n_e remains approximately constant in time. Following particle accelerator conventions, the longitudinal $\hat{z}$ axis is aligned with the motion of the electron and ion beams, while the $\hat{x}$ and $\hat{y}$ axes span the transverse plane. The transverse electron temperature typically differs from the longitudinal temperature, but we can reasonably assume cylindrical symmetry in velocity space and, hence, align the $\hat{x}$ axis with the transverse component of the ion velocity. This is why our assumed ion velocity vector has no y component.

For cold electrons and $v_{ion}\tau \gg \rho$, the ion sweeps out an approximately cylindrical volume, $V_{cold} \approx v_{ion}\tau\pi\rho^2$, where $v_{ion} =| \mathbf{v}_{ion} |= (v_{ion,x}^2 + v_{ion,z}^2)^{1/2}$. The probability that k electrons will be found in this volume is governed by Poisson statistics, with the following probability function [12]:

$$f_k = \frac{\lambda^k}{k!}e^{-\lambda}, \tag{A.1}$$

where $\lambda = n_e V_{cold}$ is the mean value.

It is convenient to work in the Galilean frame where the ion is stationary. We assume without loss of generality that the ion lies at the origin, and we consider a sphere of radius ρ that is centered on the origin. We need to know the volume of space that contains, at time $t = 0$, all electrons with trajectories that will lie inside or intersect the sphere around the ion during the time interval $0 < t < \tau$. For cold electrons, this volume is obtained by sweeping the sphere along a line of length $v_{ion}\tau$, with no dependence on the direction of the velocity vector. The resulting volume is approximately equal to V_{cold} calculated above.

For a finite electron temperature, more electrons will enter or pass through the box in time τ, which means they will also have a distance of closest approach that is $\leqslant \rho$. To include these electrons correctly in our volume calculation, we assume they all follow straight line trajectories in our Galilean frame with relative velocity $\mathbf{v}_{rel} = (-v_{ion,x} + v_{e,x}, v_{e,y}, -v_{ion,z} + v_{e,z})$. The finite-temperature volume is then found by integrating V_{cold} over the thermal electron distribution

$$f(\mathbf{v}_e) = \frac{1}{(2\pi)^{3/2}\Delta_x\Delta_y\Delta_z}\exp\left(-\frac{v_x^2}{2\Delta_x^2} - \frac{v_y^2}{2\Delta_y^2} - \frac{v_z^2}{2\Delta_z^2}\right), \tag{A.2}$$

where Δ_α is the rms value of electron velocity component v_α. This is equivalent to replacing v_{ion} in the cold formula with $\langle v_{\text{rel}}\rangle$, where $v_{\text{rel}} = |\mathbf{v}_{\text{rel}}|$:

$$\langle v_{\text{rel}}\rangle(\Delta_x, \Delta_y, \Delta_z) = \int_{-\infty}^{\infty} \mathrm{d}^3\mathbf{v}_e f(\mathbf{v}_e) \mid \mathbf{v}_{\text{rel}} \mid, \tag{A.3}$$

yielding $V_{\text{warm}} \approx \langle v_{\text{rel}}\rangle \tau \pi \rho^2$.

Just as is the case with Eq. (8), the integral in Eq. (A.3) must in general be done numerically. However, it is useful to have even an approximate analytical expression, so we consider the special case of an isotropic electron temperature, $\Delta_\alpha = \Delta$ for all α, and an ion moving only longitudinally, $v_{\text{ion},x} = 0$ and $v_{\text{ion},z} = v_{\text{ion}}$. In this limit, Eq. (A.3) can be evaluated analytically to obtain:

$$\langle v_{\text{rel}}\rangle = v_{\text{ion}} \left[\left(1 + \frac{\Delta^2}{v_{\text{ion}}^2}\right)\text{erf}\left(\frac{v_{\text{ion}}}{\sqrt{2}\Delta}\right) + \sqrt{\frac{2}{\pi}}\frac{v_{\text{ion}}}{\Delta} \exp\left(-\frac{v_{\text{ion}}^2}{2\Delta^2}\right) \right], \tag{A.4}$$

where $\text{erf}(u)$ is the usual error function, ranging from zero to unity as u ranges from zero to ∞. As expected, $\langle v_{\text{rel}}\rangle \to v_{\text{ion}}$ as $\Delta \to 0$. Also, $\langle v_{\text{rel}}\rangle \to (2/\pi)^{1/2}\Delta$ as $v_{\text{ion}} \to 0$. For the special case of $v_{\text{ion}} = \Delta$, $v_{\text{rel}} \approx 1.8v_{\text{ion}}$.

From Poisson statistics, we know that the "mean" $\lambda = n_e\langle v_{\text{rel}}\rangle\tau\pi\rho^2$ is the expectation value for the number of electrons to be found in the volume V_{warm} at $t = 0$. Given the above analysis, and the assumption of weakly perturbed orbits, we know that λ is equivalently the expectation value for the number of electron trajectories with impact parameters $\leqslant \rho$.

A.1. Smallest resolved impact parameter in a finite time

Fig. 1 shows the contributions to the longitudinal friction force, as a function of impact parameter, using Eq. (4), with $\delta v_\parallel$ calculated alternately (a) in the perturbative limit, and (b) analytically for two-body motion. In fact, each scattering event also gives the ion a small transverse velocity kick, but it is implicitly assumed that electron trajectories come from all angles, fully sampling both poloidal and azimuthal angles, so that the transverse velocity kicks average exactly to zero. Any transverse ion dynamics (in the absence of external electric or magnetic fields) is modeled as diffusion.

Because the number of collisions for a given range of impact parameters scales quadratically with impact parameter, there are generally very few scattering events for $\rho \sim \rho_{\text{min}}$. In a physical system, with finite electron density n_e and finite interaction time τ, there will be an impact parameter ρ_c, for which it is not valid to assume the occurrence of many electron trajectories that fully sample the range of scattering angles. The correct Coulomb logarithm to use when $\rho_c > 0$ is Λ_1 in Eq. (7), or Λ_2 of Eq. (37) which includes finite time effects as well.

We calculate ρ_c, using Poisson statistics, under the assumption that N_c electron–ion collisions with impact parameters $\leqslant \rho$ are required to adequately sample the poloidal and azimuthal scattering angles. Following the discussion at the beginning of this appendix, we simply equate N_c with the "mean" λ, then solve for ρ to obtain:

$$\rho_c = \sqrt{\frac{N_c}{\langle v_{\text{rel}}\rangle\tau\pi n_e}}. \tag{A.5}$$

For our RHIC parameters, we find good agreement with simulations, if we choose $N_c \approx 120$. This is a reasonable result, but may not be optimal for different parameters.

As is discussed in the body of this paper, an accurate simulation of the friction force requires many realizations of the same simulation parameters. One then averages these results and can use the Central Limit Theorem to estimate the uncertainty in this averaged friction force. However, this process can result in a large increase of the number of trajectories with small impact parameters. As a result, the averaging process (necessary to reduce error bars) also better resolves small impact parameters, which artificially reduces the value of ρ_c and, hence, increases the friction force. To account for this effect and correctly interpret simulation results, one must let $N_c \to N_c/N_{\text{traj}}$, where N_{traj} is the number of numerical trajectories used to represent each physical trajectory for the purpose of averaging.

For example, this is used to accurately interpret simulation results in Fig. 7. In all the numerical simulations (except when modeling the diffusion) we split each electron into $N_m = 267$ lighter electrons with the same charge to mass ratio, as described in Section 6. This effectively increases n_e by a factor of N_m, and together with eight trajectories gives $\rho_c = 5.3 \times 10^{-7}$ m. It is also important in the simulations to have a box size L that is large enough (a value of 8.0×10^{-4} m is used in all cases), because otherwise we will truncate some electrons that would have collided with an ion with a small impact parameter, which artificially reduces $\langle v_{\text{rel}}\rangle$ and by Eq. (A.5) increases ρ_c.

A.2. Validity criterion for linear plasma approximation

In a linear or weakly-coupled plasma, binary Coulomb collisions dominate over 3-body and higher n-body collisions. We define a 3-body collision to mean that two electrons are simultaneously within ρ of the ion, or closer. By "simultaneous", we mean here that the two events occur during the brief time interval $\tau \sim \rho/\langle v_{\text{rel}}\rangle$. In other words, a 3-body collision occurs

when two binary collisions happen close enough to each other that they cannot be treated as separate events. Hence, the expectation value for the number of 3-body collisions can be written as

$$\lambda_{3bdy} \approx \frac{4\pi}{3}\rho^3 n_e \qquad (A.6)$$

The probability that an ion will scatter two (or more) electrons, during a time interval short enough to violate the binary collision approximation, is given by

$$P_{\geqslant 2} = 1 - P_0 - P_1 = 1 - e^{-\lambda_{3bdy}} - \lambda_{3bdy}e^{-\lambda_{3bdy}}. \qquad (A.7)$$

For $\lambda_{3bdy} \ll 1$, one obtains $P_{\geqslant 2} \approx \lambda_{3bdy}^2/2 \ll 1$. This probability is order unity when λ_{3bdy} is order unity, which by definition occurs when ρ equals the Wigner-Seitz radius a. As long as the condition $\rho_{\min} \ll a$ is satisfied, we know that scattering events with impact parameter $\rho \approx a$ are very small angle and can be treated perturbatively, which means there's no coupling between nearby collisions and so the binary collision approximation remains valid. The condition $\rho_{\min} \ll a$ is equivalent to requiring that $\Lambda \gg 1$.

Appendix B. Binary Coulomb collision (BCC) algorithm details

In the BCC algorithm we solve the classical two-body, central-force problem in 3D, Eq. (32). This is a classical problem in celestial mechanics [20] and the solution is well known for attractive bodies. In our case we may have particles that repel, which is usually not considered. Therefore, we give some detail for both cases here (see Appendix Table B.1).

In this section we use $\mathbf{x}$ for the 3D position of the reduced particle Eq. (32), rather than $\mathbf{e}_{ij}$. The Lagrangian for the reduced one-particle system under a central force is

$$L = \frac{1}{2}\mu|\dot{\mathbf{x}}|^2 - V(|\mathbf{x}|), \quad \text{where } V(r) = -\frac{k}{r}.$$

By conservation of angular momentum, the motion lies in the plane defined by the initial position $\mathbf{x}_0$ and velocity $\dot{\mathbf{x}}_0 = \mathbf{v}_0$. To solve exactly, we proceed using the following steps:

(1) Find an orthonormal coordinate system $\{\mathbf{n}_1, \mathbf{n}_2, \mathbf{n}_3\}$ such that the particle motion lies in the $\mathbf{n}_1 - \mathbf{n}_2$ plane.
(2) Convert the 2D problem to polar coordinates.
(3) Solve this 2-body problem in 2D.
(4) Convert deviations from Polar to 2D Cartesian coordinates in the $\mathbf{n}_1 - \mathbf{n}_2$ plane.
(5) Convert the coordinate and velocity deviations back to 3D.

Step 1: We obtain the orthonormal coordinate system by

$$\mathbf{n}_1 = \frac{\mathbf{x}_0}{|\mathbf{x}_0|}, \qquad (B.1)$$

$$\mathbf{n}_2 = \frac{[\mathbf{x}_0 \times \mathbf{v}_0] \times \mathbf{x}_0}{|\mathbf{x}_0 \times \mathbf{v}_0||\mathbf{x}_0|} = \mathbf{n}_3 \times \mathbf{n}_1, \qquad (B.2)$$

$$\mathbf{n}_3 = \frac{\mathbf{x}_0 \times \mathbf{v}_0}{|\mathbf{x}_0 \times \mathbf{v}_0|} = \mathbf{n}_1 \times \mathbf{n}_2. \qquad (B.3)$$

If $\mathbf{v}_0 = \mathbf{0}$, or $\mathbf{v}_0$ is parallel to $\mathbf{x}_0$, the motion is 1-dimensional, but $\mathbf{n}_2$ and $\mathbf{n}_3$ are undefined. In this case $\mathbf{n}_2$ and $\mathbf{n}_3$ are not needed to calculate the motion, but we can choose $\mathbf{n}_2$ as any vector perpendicular to $\mathbf{n}_1$, and $\mathbf{n}_3 = \mathbf{n}_1 \times \mathbf{n}_2$.

Step 2: The initial position of the particle is aligned along the $\mathbf{n}_1$-axis, so in polar coordinates its initial position and velocity are:

$$r_0 = |\mathbf{x}_0|, \qquad (B.4)$$
$$\theta_0 = 0, \qquad (B.5)$$
$$\dot{r}_0 = \mathbf{v}_0 \cdot \mathbf{n}_1 = \frac{\mathbf{x}_0 \cdot \mathbf{v}_0}{|\mathbf{x}_0|}, \qquad (B.6)$$
$$\dot{\theta}_0 = \frac{\mathbf{v}_0 \cdot \mathbf{n}_2}{|\mathbf{x}_0|} = \frac{|\mathbf{x}_0 \times \mathbf{v}_0|}{|\mathbf{x}_0|^2}. \qquad (B.7)$$

Table B.1
Summary of orbit types

	$k > 0; E < 0$	$k > 0; E > 0$	$k < 0; E > 0$
Force	Attractive	Attractive	Repulsive
Orbit type	Elliptic	Hyperbolic	Hyperbolic
Eccentricity	$0 < \epsilon < 1$	$\epsilon \geqslant 1$	$\epsilon \geqslant 1$
Eccentric anomaly ψ	$r/\rho_{\min} = 1 - \epsilon\cos\psi$	$r/\rho_{\min} = \epsilon\cosh\psi - 1$	$r/\rho_{\min} = \epsilon\cosh\psi + 1$
Kepler equation	$\omega h = \psi - \epsilon\sin\psi$	$\omega h = \epsilon\sinh\psi - \psi$	$\omega h = \epsilon\sinh\psi + \psi$

Step 3: We now have a single particle of mass μ under a central force with initial conditions specified by Eqs. (B.4)–(B.7). Let $(r(t), \theta(t))$ be the exact solution to this 2-body problem, when we refer to r or θ (at an unspecified time) it will be assumed to be at the final time $t = h$. What we really need for Eqs. (30) and (31) is the change in position and velocity, and it is more efficient to calculate this difference directly rather than subtracting the nearly equal initial and final values,

$$\Delta r = r - r_0, \tag{B.8}$$
$$\Delta \theta = \theta, \tag{B.9}$$
$$\Delta \dot{r} = \dot{r} - \dot{r}_0, \tag{B.10}$$
$$\Delta \dot{\theta} = \dot{\theta} - \dot{\theta}_0. \tag{B.11}$$

There are two constants to the motion, the angular momentum ℓ and total energy E

$$\ell = \mu r^2 \dot{\theta}, \tag{B.12}$$
$$E = \frac{\mu}{2}(\dot{r}^2 + r^2\dot{\theta}^2) + V(r) = \frac{1}{2}\mu\dot{r}^2 + \frac{\ell^2}{2\mu r^2} - \frac{k}{r}. \tag{B.13}$$

We note that if $E > 0$, the orbit is hyperbolic, and $\rho = |\mathbf{x}_0 \times \mathbf{v}_0| / |\mathbf{v}_0| = |\ell|(2\mu(E + k/r))^{-1/2}$ is the classical impact parameter.

We define two dimensionless constants: η – the ratio of the semi-minor to the semi-major axis of the orbit, and ϵ – the eccentricity:

$$\eta = \sqrt{\frac{2|E|}{\mu}}\frac{|\ell|}{|k|}, \tag{B.14}$$

$$\epsilon = \sqrt{1 + \frac{2E\ell^2}{\mu k^2}} = \begin{cases} \sqrt{1 + \eta^2} & \text{hyperbolic,} \quad E > 0, \\ \sqrt{1 - \eta^2} & \text{elliptical,} \quad E < 0. \end{cases} \tag{B.15}$$

The orbit types of circular ($E = -\mu k^2/2\ell^2$, $\epsilon = 0$) and parabolic ($E = 0$, $\epsilon = 1$) are limiting cases that do not need to be considered separately. For our simulations nearly all collisions are hyperbolic because relative velocities are large. We include the elliptic solutions in what follows for completeness, and to handle its occasional occurrence.

We can now calculate r at the final time $t = h$ by solving Eq. (B.13) for $\dot{r}$ and integrating, which gives

$$h = \int_{r_0}^{r} \frac{\mu r \, \mathrm{d}r}{\sqrt{2\mu E r^2 + 2\mu k r - \ell^2}}. \tag{B.16}$$

Eq. (B.16) can be solved exactly using a change of variables involving a quantity ψ, the "eccentric anomaly". The substitutions for each case are

$$r = \rho_{\min}(\epsilon \cosh\psi - \mathrm{sgn}\,k) \quad \text{hyperbolic,} \tag{B.17}$$
$$r = \rho_{\min}(1 - \epsilon \cos\psi) \quad \text{elliptical,} \tag{B.18}$$

where $\rho_{\min} = |k/(2E)|$ is the impact parameter for a 90° collision with total energy E. The value of r_0 determines ψ_0, up to sign. It is important to set the sign of ψ_0 correctly. ψ is a time-like variable which is less than zero when $\dot{r} < 0$ and greater than zero when $\dot{r} > 0$. Therefore, we set the sign of ψ_0 to match the sign of $\dot{r}_0$. Note that $\Delta\psi$ is always positive.

ψ is the solution to the classical Kepler equation of the form:

$$\omega h = [\epsilon \sinh\psi - (\mathrm{sgn}\,k)\psi]_{\psi_0}^{\psi} \quad \text{hyperbolic,} \tag{B.19}$$
$$\omega h = [\psi - \epsilon \sin\psi]_{\psi_0}^{\psi} \quad \text{elliptical,} \tag{B.20}$$

where $\omega = \sqrt{|k|/(\mu\rho_{\min}^3)}$, or in terms of $\Delta\psi = \psi - \psi_0$,

$$\epsilon \sinh(\psi_0 + \Delta\psi) - (\mathrm{sgn}\,k)\Delta\psi = \omega h + \epsilon \sinh\psi_0, \quad \text{hyperbolic,} \tag{B.21}$$
$$\Delta\psi - \epsilon \sin(\psi_0 + \Delta\psi) = \omega h - \epsilon \sin\psi_0, \quad \text{elliptical.} \tag{B.22}$$

Note the sign difference for the opposite-sign ($k > 0$) versus like-sign ($k < 0$) particles. The Kepler equation cannot be solved analytically, but ψ can be calculated using root finding methods. In general $\Delta\psi$ is small, and we have found a good way to solve the Kepler equation is to use a few iterations of Newton's method starting with an initial guess $\Delta\psi = 0$. The Kepler equations have only a single root, and Newton's method converges to it provided $\Delta\psi$ is small. For strong collisions we can use an initial guess $\Delta\psi$ obtained by solving the Kepler Eqs. (B.21) or (B.22) after dropping the term linear in $\Delta\psi$.

After $\Delta\psi$ is determined by Eqs. (B.21) or (B.22), we substitute it back into Eqs. (B.17) or (B.18) to find Δr. This can be written to minimize cancellation of nearly equal terms by using trigonometric angle sum formulas, to yield

$$\Delta r = \begin{cases} \epsilon\rho_{\min}(\cosh\psi_0(\cosh\Delta\psi - 1) + \sinh\psi_0\sinh\Delta\psi) & \text{hyperbolic,} \\ \epsilon\rho_{\min}(\cos\psi_0(1 - \cos\Delta\psi) + \sin\psi_0\sin\Delta\psi) & \text{elliptical.} \end{cases}$$

We then calculate $\Delta\theta$ using

$$\Delta\theta = \begin{cases} \tan^{-1}\left(\frac{\eta\sinh\psi}{\epsilon-\mathrm{sgn}k\cosh\psi}\right) - \tan^{-1}\left(\frac{\eta\sinh\psi_0}{\epsilon-\mathrm{sgn}k\cosh\psi_0}\right) & \text{hyperbolic,} \\ \tan^{-1}\left(\frac{\eta\sin\psi}{\cos\psi-\epsilon}\right) - \tan^{-1}\left(\frac{\eta\sin\psi_0}{\cos\psi_0-\epsilon}\right) & \text{elliptical.} \end{cases} \tag{B.23}$$

As an aside, by considering an entire hyperbolic orbit ($\psi_0 \to -\infty$ and $\psi \to \infty$), we can use Eq. (B.23) to derive the total scattering angle given in Eq. (5). If $\Delta\Theta$ is the total change in angle over the entire orbit we have from Eq. (B.23),

$$\tan\left(\frac{\Delta\Theta}{2}\right) = -(\mathrm{sgn}k)\eta = -(\mathrm{sgn}k)\frac{\rho}{\rho_{\min}}.$$

The scattering angle $\phi = \pi - \Delta\Theta$, so that $\tan(\phi/2) = \tan(\Delta\Theta/2)^{-1}$ which gives Eq. (5). For a small time step h, Eq. (B.23) involves the difference between nearly equal quantities, it may be calculated more accurately by taking the tangent of both sides and expanding out to

$$\tan(\Delta\theta) = \frac{\eta[\epsilon\sinh\psi_0(\cosh\Delta\psi - 1) + (r_0/\rho_{\min})\sinh\Delta\psi]}{\eta^2\sinh\psi_0\sinh\psi + (\epsilon - \mathrm{sgn}k\cosh\psi_0)(\epsilon - \mathrm{sgn}k\cosh\psi)},$$

in the hyperbolic case and

$$\tan(\Delta\theta) = -\frac{\eta[\epsilon\sin\psi_0(\cos\Delta\psi - 1) - (r_0/\rho_{\min})\sin\Delta\psi]}{\eta^2\sin\psi_0\sin\psi + (\epsilon - \cos\psi_0)(\epsilon - \cos\psi)},$$

in the elliptic case. We can now obtain the velocity changes $\Delta\dot{r}$ and $\Delta\dot{\theta}$ using conservation of energy Eq. (B.13) and angular momentum Eq. (B.12), respectively.

Step 4: This is a standard coordinate transformation, except that we have deviations Δr, $\Delta\theta$, $\Delta\dot{r}$ and $\Delta\dot{\theta}$ rather than absolute coordinates. We calculate the 2D changes to coordinate and velocity using the formulas:

$$\Delta x = \Delta r\cos\Delta\theta + r_0(\cos\Delta\theta - 1), \tag{B.24}$$
$$\Delta y = (r_0 + \Delta r)\sin\Delta\theta, \tag{B.25}$$
$$\Delta\dot{x} = \Delta\dot{r}\cos\Delta\theta + \dot{r}_0(\cos\Delta\theta - 1) - (\dot{\theta}_0 + \Delta\dot{\theta})\Delta y, \tag{B.26}$$
$$\Delta\dot{y} = (\dot{r}_0 + \Delta\dot{r})\sin\Delta\theta + (\dot{\theta}_0 + \Delta\dot{\theta})\Delta x + \Delta\dot{\theta}r_0. \tag{B.27}$$

At this point we can calculate the quantities $\delta\mathbf{x}$ and $\delta\dot{\mathbf{x}}$ in terms of the $\{\mathbf{n}_1, \mathbf{n}_2, \mathbf{n}_3\}$ basis:

$$\delta\mathbf{x} = (\Delta x, \Delta y, 0) - h(\mathbf{v}_0 \cdot \mathbf{n}_1, \mathbf{v}_0 \cdot \mathbf{n}_2, 0), \tag{B.28}$$
$$\delta\dot{\mathbf{x}} = (\Delta\dot{x}, \Delta\dot{y}, 0). \tag{B.29}$$

Step 5: We now convert from the impulses from the $\{\mathbf{n}_1, \mathbf{n}_2, \mathbf{n}_3\}$ basis back to the original coordinate system

$$\delta\mathbf{x} = [\Delta x - h\mathbf{v}_0 \cdot \mathbf{n}_1]\mathbf{n}_1 + [\Delta y - h\mathbf{v}_0 \cdot \mathbf{n}_2]\mathbf{n}_2, \tag{B.30}$$
$$= [\Delta x]\mathbf{n}_1 + [\Delta y]\mathbf{n}_2 - h\mathbf{v}_0,$$
$$\delta\mathbf{v} = [\Delta\dot{x}]\mathbf{n}_1 + [\Delta\dot{y}]\mathbf{n}_2, \tag{B.31}$$

to be inserted into Eqs. (28) and (29).

Appendix C. Hermite algorithm details

When a constant magnetic field is present the Hermite algorithm is only 3rd-order, but we can recover 4th-order accuracy by changing the coefficients in the corrector. To see how to do this, we solve a problem using a force that depends linearly on velocity. It is easiest to do this in 1D where we do not have to worry about the cross-product $\mathbf{v} \times \mathbf{B}$. Consider the simple 1D model:

$$\ddot{x} = \alpha v = \alpha\dot{x}, \tag{C.1}$$

with initial conditions $x(0) = 1$ and $\dot{x}(0) = \alpha$. The exact solution is simply $x(t) = e^{\alpha t}$. Let us do one step of the Hermite algorithm starting from the exact values $x(0) = 0$, $v(0) = \alpha$, $a(0) = \alpha^2$ and $J(0) = \alpha^3$. First, the predictors Eqs. (16) and (17) give us

$$x_i^p = 1 + h\alpha + \frac{h^2}{2}\alpha^2 + \frac{h^3}{6}\alpha^3, \tag{C.2}$$
$$v_i^p = \alpha + h\alpha^2 + \frac{h^2}{2}\alpha^3, \tag{C.3}$$

which are correct to 3rd, and 2nd-order in h, respectively. We now obtain estimates for the acceleration and jerk at the next time step using Eqs. (13) and (14). Here it is important to evaluate the "field" (αv) at the predicted positions and velocities.

$$a_{1,i} = \alpha v_i^p = \alpha^2 + h\alpha^3 + \frac{h^2}{2}\alpha^4, \tag{C.4}$$

$$J_{1,i} = \alpha a_{1,i} = \alpha^3 + h\alpha^4 + \frac{h^2}{2}\alpha^5. \tag{C.5}$$

Note that these estimates are only correct up to $O(h^2)$, which is the root of the problem. Plugging these values into the estimates for snap and crackle, Eqs. (22) and (22) gives:

$$S_{0,i} = \alpha^4 - h\alpha^5, \tag{C.6}$$

$$C_{0,i} = 3\alpha^5. \tag{C.7}$$

These equations signal a problem, because as the fourth and fifth derivatives at $t = 0$, we need $S_{0,i} = \alpha^4 + O(h^2)$ and $C_{0,i} = \alpha^5 + O(h)$. If we blindly substitute these values into the corrector Eqs. (24) and (25), we will get

$$x_i(t + h) = x_i^p + \frac{h^4}{24}\alpha^4 - \frac{2h^5}{120}\alpha^5, \tag{C.8}$$

$$v_i(t + h) = v_i^p + \frac{h^3}{6}\alpha^4 - \frac{h^4}{24}\alpha^5. \tag{C.9}$$

These two equations are correct only to 4th-order, and 3rd-order, respectively, because the coefficients in front of the α^5 terms should be $+1/120$ and $+1/24$. If we implement the Hermite algorithm in this simple way it will only be 3rd-order accurate in h.

The good news is that this problem is easily corrected, at least when the external force depends linearly on velocity. The first technique is to note that linear combinations of $S_{0,i}$ and $C_{0,i}$ give the terms we want, i.e.

$$S'_{0,i} = S_{0,i} + h\frac{C_{0,i}}{3} = -2\frac{(a_{0,i} - a_{1,i}) + hJ_{0,i}}{h^2} = \alpha^4 + O(h^2), \tag{C.10}$$

$$C'_{0,i} = \frac{C_{0,i}}{3} = 2\frac{2(a_{0,i} - a_{1,i}) + h(J_{0,i} + J_{1,i})}{h^3} = \alpha^5 + O(h). \tag{C.11}$$

We see that these new estimates of snap and crackle have the correct orders, and if we use them in the correctors, Eqs. (24) and (25), we will get a 4th-order scheme. Equivalently, we can use the old values of $S_{0,i}$ and $C_{0,i}$, but choose corrector coefficients a_1 and a_2 such that

$$\frac{h^4}{24}S_{0,i} + a_1 h^5 C_{0,i} = \frac{h^4}{24}\alpha^4 + \frac{h^5}{120}\alpha^5, \tag{C.12}$$

$$\frac{h^3}{6}S_{0,i} + a_2 h^4 C_{0,i} = \frac{h^3}{6}\alpha^4 + \frac{h^4}{24}\alpha^5, \tag{C.13}$$

which, using the values for $S_{0,i}$ and $C_{0,i}$ in Eqs. (C.6) and (C.7) give $a_1 = 1/60$ and $a_2 = 5/72$. Thus, for particle position and velocity changes corresponding to the fields, the corrector becomes:

$$\mathbf{x}_i(t + h) = \mathbf{x}_i^p + \frac{h^4}{24}\mathbf{S}_{0,i} + \frac{h^5}{60}\mathbf{C}_{0,i}, \tag{C.14}$$

$$\mathbf{v}_i(t + h) = \mathbf{v}_i^p + \frac{h^3}{6}\mathbf{S}_{0,i} + \frac{5h^4}{72}\mathbf{C}_{0,i}. \tag{C.15}$$

References

[1] S.J. Aarseth, Direct methods for N-body simulations, in: J.U. Brackbill, B.I. Cohen (Eds.), Multiple Time Scales, Academic Press, New York, 1985, p. 377.
[2] G.I. Bell, D.L. Bruhwiler, V.N. Litvinenko, R. Busby, D.T Abell, P. Messmer, S. Veitzer, J.R. Cary, Simulations of dynamical friction including spatially-varying magnetic fields, in: S. Nagaitsev, R.J. Pasquinelli (Eds.), Beam Cooling and Related Topics, AIP Conference Proceedings 821, 329, 2006.
[3] G.I. Bell, D.L. Bruhwiler, A. Sobol, I. Ben-Zvi, A. Fedotov, V. Litvinenko, Numerical algorithms for modeling electron cooling in the presence of external fields, in: Proceedings of the Particle Acceleration Conference, Albuquerque, June, 2007, p. 3549.
[4] I. Ben-Zvi et al. Status of the R&D Towards Electron Cooling of RHIC, in: Proceedings of the Particle Acceleration Conference, Albuquerque, June, 2007, p. 1938.
[5] J. Boris, in: Proceedings of the Fourth Conference on Numerical Simulation of Plasmas, J.P. Boris, R.A. Shanny (Eds.), Naval Research Laboratory, Washington, DC, 1970, p. 367.
[6] D.L. Bruhwiler, R. Busby, A.V. Fedotov, I. Bev-Zvi, J.R. Cary, P. Stoltz, A. Burov, V.N. Litvinenko, P. Messmer, D. Abell and C. Nieter, Direct simulation of friction forces for heavy ions interacting with a warm magnetized electron distribution, in: AIP Conference Proceedings 773 Bensheim, Germany, 2004, p. 394.
[7] G.I. Budker, At. Energy 22 (1967) 346.
[8] J.D. Callen, Fundamentals of Plasma Physics, online book available at <http://homepages.cae.wisc.edu/~callen>.
[9] S. Chandrasekhar, Principles of Stellar Dynamics, University of Chicago Press, 1942.
[10] Ya. Derbenev, A. Skrinsky, Part. Acc. 8 (1978) 235.
[11] Ya. Derbenev, Electron cooling of heavy ions in solenoid with undulator (TJLAB Note), unpublished.
[12] M. Evans, N. Hastings, B. Peacock, Statistical Distributions, 2nd ed., John Wiley and Sons, New York, 1993 (Chapter 31).
[13] A.V. Fedotov, I. Ben-Zvi, V.N. Litvinenko, A. Sidorin, A. Smirnov, G. Trubnikov, Proceedings of the PAC05 Conference, Knoxville, TN, 2005, p. 4236.

[14] A.V. Fedotov, D.L. Bruhwiler, A.O. Sidorin, D.T. Abell, I. Ben-Zvi, R. Busby, J.R. Cary, V.N. Litvinenko, Numerical study of the magnetized friction force, Phys. Rev. ST/AB 9 074401 (2006).
[15] A.V. Fedotov, I. Ben-Zvi, D.L. Bruhwiler, V.N. Litvinenko, A.O. Sidorin, High-energy electron cooling in a collider, New J. Phys. 8 (2006) 283.
[16] A.V. Fedotov, D.L. Bruhwiler, D.T. Abell, A.O. Sidorin, Detailed studies of electron cooling friction force, in: S. Nagaitsev, R.J. Pasquinelli (Eds.), Beam Cooling and Related Topics, AIP Conference Proceedings 821, 2006, p. 319.
[17] A.V. Fedotov, I. Ben-Zvi, D. Kayran, V.N. Litvinenko, E. Pozdeyev, G. Bell, D.L. Bruhwiler, A. Sobol, A. Sidorin, A. Smirnov, Electron cooling in the presence of undulator fields, Particle Accelerator Conference, Albuquerque, June, 2007, p. 3696.
[18] W. Fischer, Magnetic field error coefficients for helical dipoles, BNL Report# RHIC/AP/83, January 1996.
[19] H.P. Freund, T.M. Antonsen Jr., Principles of Free-electron Lasers, Chapman & Hall, 1992.
[20] H. Goldstein, Classical Mechanics, 2nd ed., Addison-Wesley, 1980 (Chapter 3).
[21] M. Larsson, Rep. Prog. Phys. 58 (1995) 1267.
[22] J. Makino, S.J. Aarseth, On a Hermite integrator with Ahmad–Cohen scheme for gravitational many-body problems, Publ. Astron. Soc. Jpn. 44 (1992) 14.
[23] I.N. Meshkov, Nucl. Instrum. Methods Phys. Res. Sect. A 391 (1997) 1.
[24] S. Nagaitsev, D. Broemmelsiek, A. Burov, et al, Experimental demonstration of relativistic electron cooling, Phys. Rev. Lett. 96 (2006) 044801.
[25] C. Nieter, J.R. Cary, VORPAL: a versatile plasma simulation code, J. Comput. Phys. 196 (2004) 448.
[26] V.V. Parkhomchuk, A.N. Skrinsky, Rep. Prog. Phys. 54 (1991) 919.
[27] A.O. Sidorin, I.N. Meshkov, I.A. Seleznev, A.V. Smirnov, E.M. Syresin, G.V. Trubnikov, Nucl. Instrum. Methods Phys. Res., Sect. A 558, 325 (2006) <http://lepta.jinr.ru>.
[28] B.A. Trubnikov, Rev. Plasma Phys. 1 (1965) 105.
[29] G. Zwicknagel, C. Toepffer, P.-G. Reinhard, Stopping of heavy ions in plasmas at strong coupling, Phys. Rep. 309 (1999) 117.
[30] G. Zwicknagel, C. Toepffer, P.-G. Reinhard, Erratum, Phys. Rep. 314 (1999) 671.